Estimates of exchange topological contributions and *CP*-violating observables in $\Lambda_b \to \Lambda\phi$ decay

Zhou Rui,* Jia-Ming Li, and Chao-Qi Zhang

College of Sciences, North China University of Science and Technology, Tangshan 063009, China

(Received 16 January 2023; accepted 16 March 2023; published 30 March 2023)

The penguin-dominated two-body weak decay of $\Lambda_b \to \Lambda\phi$ is studied based on the perturbative QCD approach. In addition to the penguin emission diagrams, the penguin exchange and W exchange ones are also accounted for. It is found that the penguin exchange contribution is in fact important and comparable to the penguin emission one, while the W exchange contribution is highly Cabibbo-Kobayashi-Maskawa (CKM) suppressed. The predicted branching ratio, $\mathcal{B}(\Lambda_b \to \Lambda\phi) = 6.9^{+1.9+1.8}_{-2.0-1.6} \times 10^{-6}$, is larger than the previous theoretical estimates but in comparison with the data from Particle Data Group at the level of 1 standard deviation. We also explore some pertinent decay asymmetry parameters that characterize the angular decay distributions. The inclusion of the W exchange contribution provides the nonzero weak phase difference, consequently, allowing us to estimate the direct CP violation and true triple product asymmetries in the concerned process. The numerical results demonstrate that the direct CP violation is at the level of a few percent, and the true triple product asymmetries are also predicted to be tiny, of order 10^{-2}–10^{-4}. The observed small CP-violating observables have shown no significant deviations from zero. Our predictions will be subject to stringent tests with precise data from LHCb in the future.

DOI: 10.1103/PhysRevD.107.053009

I. INTRODUCTION

With huge statistics of beauty hadrons were accumulated at the high energy and high intensity of the Large Hadron Collider (LHC), several charmless Λ_b decays of final states containing Λ have been measured to be of order of 10^{-6} with good precision [1–6]. After the evidence has been reported for the $\Lambda_b \to \Lambda\eta$ decay [4], the first vector mode $\Lambda_b \to \Lambda\phi$ was observed with a significance of 5.9 standard deviations by the LHCb Collaboration in 2016 [5]. Some triple product asymmetries (TPAs) were measured to be consistent with zero and no CP violation was found. The current world average of its branching ratio given by Particle Data Group (PDG) [7] is $(9.8 \pm 2.6) \times 10^{-6}$, where multiple uncertainties are added in quadrature. These measurements are crucial for an in-depth understanding of the strong dynamics in the b-baryon decays.

Fueled by these observations, theoretical interests on the $\Lambda_b \to \Lambda\phi$ mode were increased recently. In Ref. [8], the authors studied the nonleptonic two-body decays of Λ_b within the QCD factorization approach (QCDF) under the diquark hypothesis, in which the two light spectator quarks in baryon are considered as a scalar of color antitriplet. This approximation may work well for the processes where the W emission contribution is dominant. However, for the processes where the diquark is broken during the transition, such as the exchange topological contributions, the plausibility of the diquark scenario may encounter serious challenges. As the predicted branching ratio of the $\Lambda_b \to \Lambda\phi$ decay from [8] is an order of magnitude smaller than the experimental value, the reasonability of the diquark hypothesis in this mode needs to be further tested. The process $\Lambda_b \to \Lambda\phi$ was also addressed in [9,10] by using the generalized factorization approach (GFA), in which the nonfactorizable contributions are parametrized in terms of the effective number of colors $N_c^{\rm eff}$. The obtained branching ratio with $N_c^{\rm eff} = 2$ was matched to the LHCb measurement, which implies the sizeable nonfactorizable effects in the decay under consideration. Very recently, the angular analyses for $\Lambda_b \to \Lambda V$ with V being a light vector meson has been derived in GFA [11], in which the T-violating observables were explored systematically. Further information on this rich subject in the baryon sector may be found in Refs. [12–20].

Above theoretical studies are performed by the factorization ansatz, within which the contributions from the

*Corresponding author.
jindui1127@126.com

factorizable emission diagrams for the color-allowed decays can be estimated reliably. Nonetheless, the nonfactorizable effects, especially from the W and penguin exchange diagrams, still cannot be well explored. As stated in [21–24], contrary to the meson case, the W exchange contribution plays a dramatic role in baryon decays on account of the fact that it is neither helicity nor color suppressed since there may exist a scalar isosinglet diquark inside the baryon. Experimentally the observation of the W-exchange-only processes $\Lambda_c^+ \to \Xi^0 K^+, \Delta^{++} K^-$ [7,25] with a surprisingly large branching ratios indicates that W exchange indeed plays an essential role in charmed baryon decays. As of today, many efforts have been made to estimate the W exchange contributions to the baryon decays using phenomenological models such as spectator quark model [23], the pole model approach [26–31], the current-algebra approach [22,30,32–34], final-state interaction rescattering [35,36], the topological diagram approach [37], and constituent quark model [38]. All of these theoretical studies show that nonfactorizable W exchange effects are generally important in the weak decays of singly and doubly charm baryons. Recently, it was also observed that the W exchange contribution is in fact not negligible in the charmful two-body baryonic B decays [39]. This begs the question of whether W exchange effects are important in bottom baryon decays, which have received less attention in the literature except those in Refs. [40–42].

In the bottom baryon sector, the significant W exchange contribution in the exclusive nonleptonic bottom to charm baryon decays was observed to be as important as the nonfactorizable W emission one based on the relativistic three-quark model [40,41]. In the decay $\Lambda_b \to \Lambda_c \pi$, the total contribution of the nonfactorizable diagrams can amount to 30% of the factorizable contribution in amplitude. Nevertheless, the discussion in [40,41] is only limited to the Cabibbo-favored decays mediated by the tree type transition $b \to c\bar{u}d$ with a light pseudoscalar meson in the final state. Very recently, the W exchange contribution has been studied in some hadronic decays of bottom baryon [42], where the initial and final state baryons belong to different isospin representations and any factorizable amplitude is forbidden. It will be of great interest to examine how substantial these nonfactorizable effects are in the penguin-dominated processes. On the other hand, it is well known that the T-odd observables vanish in the penguin-dominated decays induced by a single weak $b \to s$ transition. However, after considering W exchange tree amplitudes, they could interfere with the penguin amplitudes, and produce the nonzero values of true T-violating observables, which could be measured in the experiments.

The perturbative QCD (PQCD) approach has been developed and successfully applied to deal with weak decays of Λ_b baryon [43–49], in which various contributions, such as emission and exchange ones, can be evaluated in a self-consistent manner. We previously investigated the color-allowed $\Lambda_b \to \Lambda_c(\pi, K)$ decays [50] and the color-suppressed $\Lambda_b \to \Lambda(J/\psi, \psi(2S))$ decays [51] within this approach and obtained satisfactory results. In this work, we will analyze the two-body $\Lambda_b \to \Lambda\phi$ decay in the PQCD approach to the leading order in the strong coupling α_s expansion. The decay under consideration is the penguin-dominated mode induced by the neutral-current $b \to s$ transition, which also receive tree diagram contributions from the W exchange diagrams via $bu \to su$ transition. The decay amplitudes include the contributions from the penguin emission, penguin exchange, as well as W exchange diagrams. The last two contributions were not considered in previous studies. By explicitly calculating this process, we shall demonstrate that the penguin exchange diagrams in fact give contribution of the same order as that from penguin emission ones, while the W exchange contribution is highly CKM suppressed. Aside from the decay branching ratio, many asymmetries derived from the angular distribution are also predicted and compared with other theoretical results and experiments. In particular, we give the theoretical predictions on the TPAs in $\Lambda_b \to \Lambda\phi$ decay for the first time, which could be checked by future experiments.

The rest of the paper is organized as follows. After presenting the effective hamiltonian, kinematics, and the light-cone distribution amplitudes (LCDAs) in Sec. II, we give a general PQCD formalism for $\Lambda_b \to \Lambda\phi$, which can be applied to other $\Lambda_b \to \Lambda V$ decays. The numerical results for the invariant and helicity amplitudes, decay branching ratio, various asymmetries, and CP-violating observables are presented in Sec. III. Finally, Sec. IV will be the conclusion of this work. Some details of the factorization formulas are displayed in the Appendix.

II. THEORETICAL FRAMEWORK

A. Hamiltonian and kinematics

In the standard model (SM), $\Lambda_b \to \Lambda\phi$ involving $b \to s$ transition is governed by the following effective Hamiltonian [52]

$$\mathcal{H}_{\text{eff}} = \frac{G_F}{\sqrt{2}} \left(V_{ub} V_{us}^* [C_1(\mu) O_1(\mu) + C_2(\mu) O_2(\mu)] - \sum_{k=3}^{10} V_{tb} V_{ts}^* C_k(\mu) O_k(\mu) \right) + \text{H.c.}, \tag{1}$$

with the Fermi coupling constant G_F. V_{ij} are the related Cabibbo-Kobayashi-Maskawa (CKM) matrix elements. $C_i(\mu)$ are the Wilson coefficients evaluated at the renormalization scale μ. The effective four-quark operators O_i containing quark and gluon fields are given by

$$
\begin{aligned}
O_1 &= \bar{u}_\alpha \gamma_\mu (1-\gamma_5) b_\beta \otimes \bar{s}_\beta \gamma^\mu (1-\gamma_5) u_\alpha, \\
O_2 &= \bar{u}_\alpha \gamma_\mu (1-\gamma_5) b_\alpha \otimes \bar{s}_\beta \gamma^\mu (1-\gamma_5) u_\beta, \\
O_3 &= \bar{s}_\beta \gamma_\mu (1-\gamma_5) b_\beta \otimes \sum_{q'} \bar{q}'_\alpha \gamma^\mu (1-\gamma_5) q'_\alpha, \\
O_4 &= \bar{s}_\beta \gamma_\mu (1-\gamma_5) b_\alpha \otimes \sum_{q'} \bar{q}'_\alpha \gamma^\mu (1-\gamma_5) q'_\beta, \\
O_5 &= \bar{s}_\beta \gamma_\mu (1-\gamma_5) b_\beta \otimes \sum_{q'} \bar{q}'_\alpha \gamma^\mu (1+\gamma_5) q'_\alpha, \\
O_6 &= \bar{s}_\beta \gamma_\mu (1-\gamma_5) b_\alpha \otimes \sum_{q'} \bar{q}'_\alpha \gamma^\mu (1+\gamma_5) q'_\beta, \\
O_7 &= \frac{3}{2} \bar{s}_\beta \gamma_\mu (1-\gamma_5) b_\beta \otimes \sum_{q'} e_{q'} \bar{q}'_\alpha \gamma^\mu (1+\gamma_5) q'_\alpha, \\
O_8 &= \frac{3}{2} \bar{s}_\beta \gamma_\mu (1-\gamma_5) b_\alpha \otimes \sum_{q'} e_{q'} \bar{q}'_\alpha \gamma^\mu (1+\gamma_5) q'_\beta, \\
O_9 &= \frac{3}{2} \bar{s}_\beta \gamma_\mu (1-\gamma_5) b_\beta \otimes \sum_{q'} e_{q'} \bar{q}'_\alpha \gamma^\mu (1-\gamma_5) q'_\alpha, \\
O_{10} &= \frac{3}{2} \bar{s}_\beta \gamma_\mu (1-\gamma_5) b_\alpha \otimes \sum_{q'} e_{q'} \bar{q}'_\alpha \gamma^\mu (1-\gamma_5) q'_\beta,
\end{aligned} \tag{2}
$$

where $O_{1,2}$ are the current-current operators arising from W boson exchange (α, β denote colors), $O_{3,4,5,6}$ and $O_{7,8,9,10}$ are the QCD and the electroweak penguin operators, respectively. $e_{q'}$ is the electric charges of the quark q' in units of $|e|$. The sum over q' runs over the quark fields active at the b quark mass scale, i.e., $q' = u, d, s, c, b$.

According to the topological classification of weak interactions, the concerned decay amplitude receives contributions from the penguin emission, W exchange, and penguin exchange diagrams as shown in Figs. 1, 2, and 3, respectively. The emission diagrams shown in Fig. 1 can only contribute to the decay by inserting the penguin operators, we thus call them the penguin emission diagrams marked by P. Figure 2 is manifested in the W exchange processes via $bu \to su$ transition, which can be classified into two types labeled by E and B (the last two diagrams), respectively. The former represents that the two quarks produced by the weak interaction are shared by the final state baryon and meson, while the latter denotes that both the two quarks flow into the Λ baryon. By exchanging the b and u quarks in the Λ_b baryon from the W exchange diagrams, one can obtain two corresponding penguin exchange diagrams denoted by PE and PB as exhibited in Fig. 3. We do not show those diagrams by exchanging u and d quarks in the initial and final states baryons from the previous diagrams because their amplitudes are equivalent under this interchange. In total, there are 136 Feynman diagrams, each denoted by R_{ij} with $R = P, PE, PB, E, B$ and the subscript ij representing possible ways of exchanging two hard gluons. It is worth to underline that in the B and PB type diagrams, the $s\bar{s}$ pair must attach two gluons to form a color singlet ϕ meson. Since the fermion flows of the diagrams $PE(PB)$ and $E(B)$ type can be converted into each other via the Fierz transformation, we insert the tree operators into E and B type diagrams and the penguin operators into PE and PB ones in the following analysis to avoid counting these contributions repetitively.

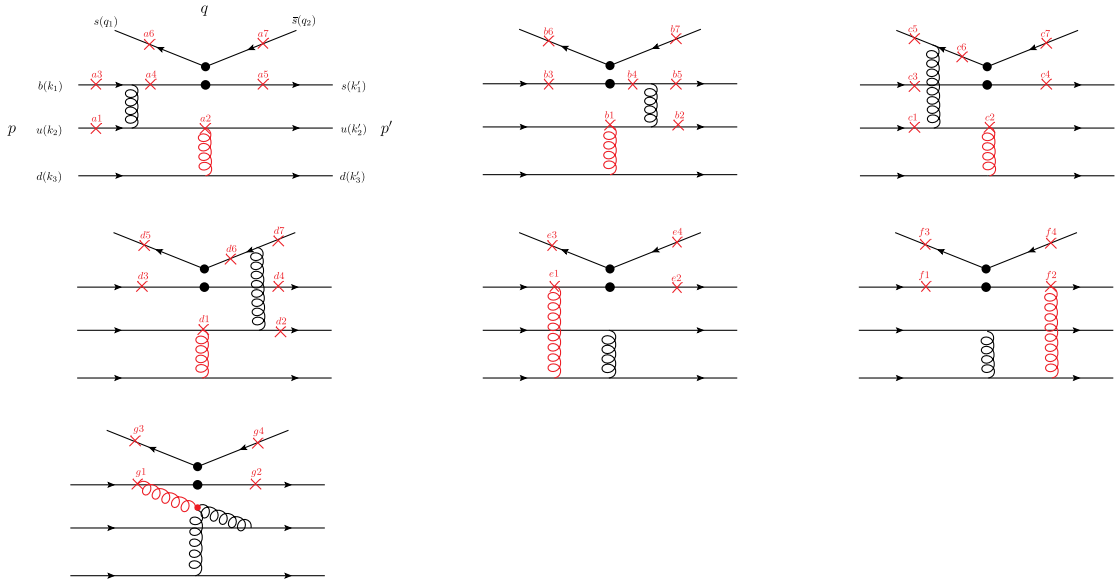

FIG. 1. Penguin emission (P) diagrams for the $\Lambda_b \to \Lambda\phi$ decay to the lowest order in the PQCD approach, where the solid black blob represents the vertex of the effective weak interaction. The crosses on the quark lines, indicated by ij with $i = a$–f and $j = 1$–7, denote the possible ways in which the quark is connected to the spectator d quark via a hard gluon. Those diagrams with exchanging u and d quarks in the $\Lambda_{(b)}$ baryons simultaneously, giving the identical contribution, are not displayed.

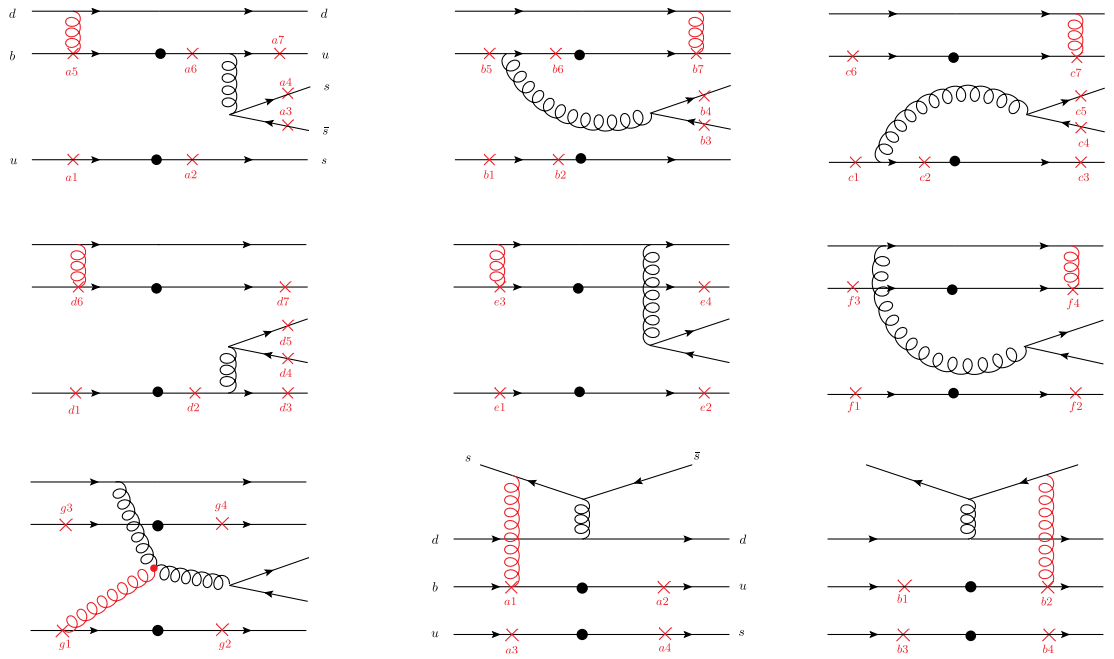

FIG. 2. W exchange diagrams for the decay $\Lambda_b \to \Lambda\phi$. The first two rows are called E-type diagrams marked by E_{ij} with $i = a$–f and $j = 1$–7. The first diagram in the third row is the three-gluon E-type marked by E_{gj} with $j = 1$–4, while the last two diagrams are classified as bow tie type W exchange diagrams marked by B_{ij} with $i = a$, b and $j = 1$–4.

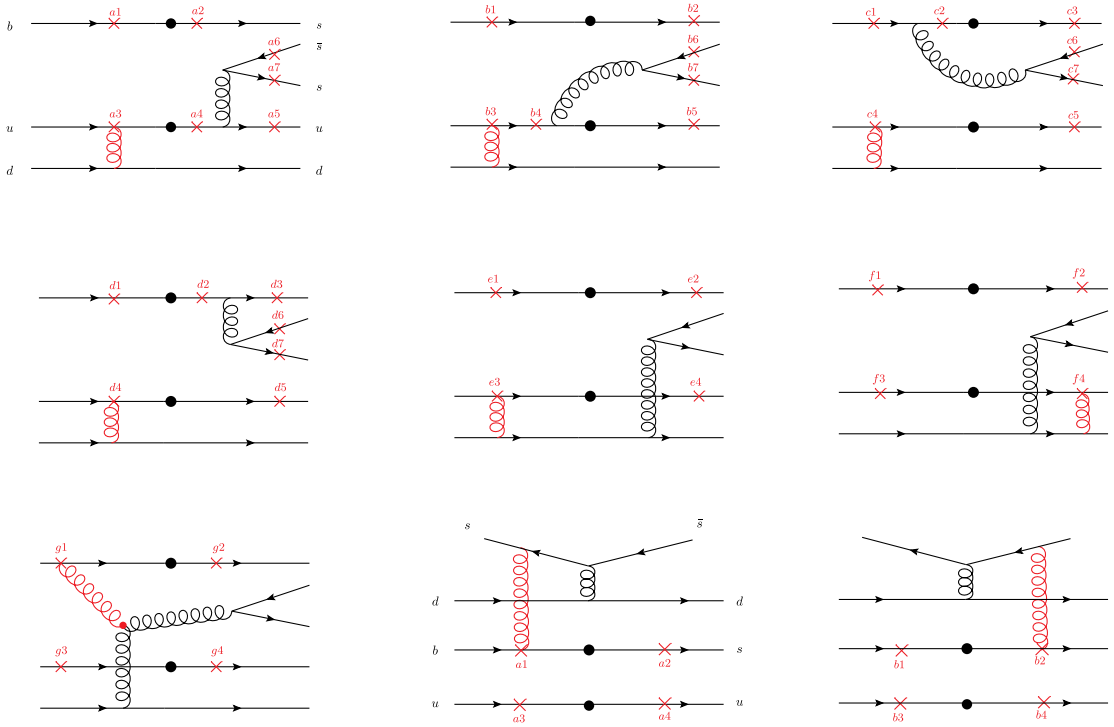

FIG. 3. Penguin exchange diagrams for the decay $\Lambda_b \to \Lambda\phi$, which are similar to Fig. 2 but with the penguin operators inserting.

We shall work in the rest frame of the baryon Λ_b with the baryon Λ moving in the dominant positive direction on the light cone

$$p = \frac{M}{\sqrt{2}}(1,1,\mathbf{0}_T), \qquad p' = \frac{M}{\sqrt{2}}(f^+, f^-, \mathbf{0}_T),$$
$$q = \frac{M}{\sqrt{2}}(1-f^+, 1-f^-, \mathbf{0}_T), \tag{3}$$

with M being the Λ_b baryon mass. The factors $f^\pm$ can be derived from the on-shell conditions $p'^2 = m_\Lambda^2$ and $q^2 = m_\phi^2$ for the final-state hadrons, which yield

$$f^\pm = \frac{1}{2}\left(1 - r_\phi^2 + r_\Lambda^2 \pm \sqrt{(1-r_\phi^2+r_\Lambda^2)^2 - 4r_\Lambda^2}\right), \tag{4}$$

with the mass ratios $r_{\Lambda,\phi} = m_{\Lambda,\phi}/M$. At the end of the derivation of the factorization formulas, the terms $r_{\Lambda,\phi}^2 \sim 0.04$ in the above kinematic variables will be neglected. For the vector meson, the longitudinal and transverse polarization vectors ($\epsilon_{L,T}$) can be determined by the normalization and orthogonality conditions as

$$\epsilon_L = \frac{1}{\sqrt{2}r_\phi}(f^+ - 1, 1 - f^-, \mathbf{0}_T), \quad \epsilon_T = (0,0,\mathbf{1}_T). \tag{5}$$

The momenta of eight valence quarks in the initial and final states, whose notations are displayed in Fig. 1, are parametrized as

$$k_1 = \left(\frac{M}{\sqrt{2}}, \frac{M}{\sqrt{2}}x_1, \mathbf{k}_{1T}\right), \qquad k_2 = \left(0, \frac{M}{\sqrt{2}}x_2, \mathbf{k}_{2T}\right), \qquad k_3 = \left(0, \frac{M}{\sqrt{2}}x_3, \mathbf{k}_{3T}\right),$$
$$k_1' = \left(\frac{M}{\sqrt{2}}f^+x_1', 0, \mathbf{k}_{1T}'\right), \qquad k_2' = \left(\frac{M}{\sqrt{2}}f^+x_2', 0, \mathbf{k}_{2T}'\right), \qquad k_3' = \left(\frac{M}{\sqrt{2}}f^+x_3', 0, \mathbf{k}_{3T}'\right),$$
$$q_1 = \left(\frac{M}{\sqrt{2}}y(1-f^+), \frac{M}{\sqrt{2}}y(1-f^-), \mathbf{q}_T\right),$$
$$q_2 = \left(\frac{M}{\sqrt{2}}(1-y)(1-f^+), \frac{M}{\sqrt{2}}(1-y)(1-f^-), -\mathbf{q}_T\right), \tag{6}$$

where $x_{1,2,3}^{(\prime)}$, and y are the parton longitudinal momentum fractions and $\mathbf{k}_{1T,2T,3T}^{(\prime)}$, and $\mathbf{q}_T$ are the corresponding transverse momenta. The momentum conservation implies the relations

$$\sum_{l=1}^{3} x_l^{(\prime)} = 1, \qquad \sum_{l=1}^{3} \mathbf{k}_{lT}^{(\prime)} = 0. \tag{7}$$

B. Light-cone distribution amplitudes

In the heavy quark limit, the Λ_b baryon LCDAs can be defined as matrix elements of non-local light-ray operators [53–58]. It is more convenient to use the form in the momentum-space for practical applications, whose Lorentz structures up to twist-4 accuracy can be written as [55]

$$(\Psi_{\Lambda_b})_{\alpha\beta\gamma}(x_i,\mu) = \frac{1}{8N_c}\{f_{\Lambda_b}^{(1)}(\mu)[M_1(x_2,x_3)\gamma_5 C^T]_{\gamma\beta} + f_{\Lambda_b}^{(2)}(\mu)[M_2(x_2,x_3)\gamma_5 C^T]_{\gamma\beta}\}[\Lambda_b(p)]_\alpha, \tag{8}$$

where α,β,γ are the spinor indices. $\Lambda_b(p)$ is the Dirac spinor. N_c is the number of colors. C^T denotes the charge conjugation matrix under transpose transform. The normalization constants $f_{\Lambda_b}^{(1)} \approx f_{\Lambda_b}^{(2)} \equiv f_{\Lambda_b} = 0.021 \pm 0.004\ \mathrm{GeV}^3$ [49], which is close to the value from the leading-order sum rule calculation [59]. The chiral-even (M_1) and odd (M_2) projectors read

$$M_1(x_2,x_3) = \frac{\not{v}\not{n}}{4}\Psi_3^{+-}(x_2,x_3) + \frac{\not{n}\not{v}}{4}\Psi_3^{-+}(x_2,x_3),$$
$$M_2(x_2,x_3) = \frac{\not{n}}{\sqrt{2}}\Psi_2(x_2,x_3) + \frac{\not{v}}{\sqrt{2}}\Psi_4(x_2,x_3), \tag{9}$$

respectively, where two light-cone vectors $n = (1,0,\mathbf{0}_T)$ and $v = (0,1,\mathbf{0}_T)$ satisfy $n\cdot v = 1$. Note that the momentum of the Λ baryon is along the n direction in the massless limit. For the shape of the various twist, we use the simple exponential model [55]

$$\Psi_2(x_2,x_3) = x_2x_3\frac{M^4}{\omega_0^4}e^{-\frac{(x_2+x_3)M}{\omega_0}},$$
$$\Psi_3^{+-}(x_2,x_3) = 2x_2\frac{M^3}{\omega_0^3}e^{-\frac{(x_2+x_3)M}{\omega_0}},$$
$$\Psi_3^{-+}(x_2,x_3) = 2x_3\frac{M^3}{\omega_0^3}e^{-\frac{(x_2+x_3)M}{\omega_0}},$$
$$\Psi_4(x_2,x_3) = \frac{M^2}{\omega_0^2}e^{-\frac{(x_2+x_3)M}{\omega_0}}, \tag{10}$$

with $\omega_0 = 0.4$ GeV.

For the LCDAs of Λ baryon, we would like to adopt the Chernyak-Ogloblin-Zhitnitsky (COZ) model proposed in Ref. [60]. This choose is supported by the previous PQCD calculation on the form factors of $\Lambda_b \to \Lambda$ transition as discussed in [51]. Other available models, such as QCD sum rules and lattice QCD (LQCD), one refers to Refs. [61–66] for details. The nonlocal matrix element associated with Λ baryon at leading twist is given by [51]

$$(\Psi_\Lambda)_{\alpha\beta\gamma}(k_i',\mu) = \frac{1}{8\sqrt{2N_c}}\{(\not{p}'C)_{\beta\gamma}[\gamma_5\Lambda(p')]_\alpha\Phi^V(k_i',\mu) + (\not{p}'\gamma_5 C)_{\beta\gamma}[\Lambda(p')]_\alpha\Phi^A(k_i',\mu) + (i\sigma_{\mu\nu}p'^\nu C)_{\beta\gamma}[\gamma^\mu\gamma_5\Lambda(p')]_\alpha\Phi^T(k_i',\mu)\}, \tag{11}$$

with $\sigma_{\mu\nu} = i[\gamma_\mu,\gamma_\nu]/2$, and $\Lambda(p')$ is the Λ baryon spinor. Φ^V and Φ^T are antisymmetric under permutation of two light quarks, while Φ^A is symmetric under the same operation. Their explicit forms at the scale $\mu = 1$ GeV in the COZ model are given as [60]

$$\begin{aligned}
\Phi^V(x_1,x_2,x_3) &= 42 f_\Lambda \phi_{\rm asy}[0.18(x_2^2 - x_3^2) - 0.1(x_2 - x_3)],\\
\Phi^A(x_1,x_2,x_3) &= -42 f_\Lambda \phi_{\rm asy}[0.26(x_3^2 + x_2^2) + 0.34x_1^2 - 0.56x_2x_3 - 0.24x_1(x_2 + x_3)],\\
\Phi^T(x_1,x_2,x_3) &= 42 f_\Lambda^T \phi_{\rm asy}[1.2(x_3^2 - x_2^2) + 1.4(x_2 - x_3)],
\end{aligned} \tag{12}$$

with $\phi_{\rm asy}(x_1,x_2,x_3) = 120x_1x_2x_3$ being the asymptotic form in the limit of $\mu \to \infty$. Φ^A and Φ^T satisfy the normalizations [60]

$$\int_0^1 \Phi^A dx_1 dx_2 dx_3 \delta(1 - x_1 - x_2 - x_3) = -f_\Lambda, \qquad \int_0^1 \Phi^T x_2 dx_1 dx_2 dx_3 \delta(1 - x_1 - x_2 - x_3) = f_\Lambda^T, \tag{13}$$

respectively, where the two normalization constants are set to be $f_\Lambda = 10 f_\Lambda^T = 6.3 \times 10^{-3}$ GeV^2 [60].

For a light vector meson V, the light-cone distribution amplitudes for longitudinal (L) and transverse (T) polarizations can be written as [67–69]

$$\begin{aligned}
\Phi_V^L(y) &= \frac{1}{\sqrt{2N_c}}[m_V \not{\epsilon}_L \phi_V(y) + \not{\epsilon}_L \not{n} \phi_V^t(y) + m_V \phi_V^s(y)],\\
\Phi_V^T(y) &= \frac{1}{\sqrt{2N_c}}[m_V \not{\epsilon}_T \phi_V^v(y) + \not{\epsilon}_T \not{n} \phi_V^T(y) + i m_V \epsilon^{\mu\nu\rho\sigma}\gamma_5\gamma_\mu \epsilon_{T\nu} v_\rho n_\sigma \phi_V^a(y)],
\end{aligned} \tag{14}$$

respectively. Here $\epsilon^{\mu\nu\rho\sigma}$ is the totally antisymmetric unit Levi-Civita tensor with the convention $\epsilon^{0123} = 1$. The twist-2 LCDAs are given by

$$\begin{aligned}
\phi_V(y) &= \frac{f_V}{\sqrt{2N_c}} 3y(1-y)[1 + a_{1V}^\parallel 3(2y-1) + a_{2V}^\parallel 3(5(2y-1)^2 - 1)/2],\\
\phi_V^T(y) &= \frac{f_V^T}{\sqrt{2N_c}} 3y(1-y)[1 + a_{1V}^\perp 3(2y-1) + a_{2V}^\perp 3(5(2y-1)^2 - 1)/2],
\end{aligned} \tag{15}$$

and those of twist-3 ones for the asymptotic form are

$$\begin{aligned}
\phi_V^t(y) &= \frac{3 f_V^T}{2\sqrt{2N_c}}(2y-1)^2, \qquad \phi_V^s(y) = -\frac{3 f_V^T}{2\sqrt{2N_c}}(2y-1),\\
\phi_V^v(y) &= \frac{3 f_V}{8\sqrt{2N_c}}[1 + (2y-1)^2], \qquad \phi_V^a(y) = -\frac{3 f_V}{4\sqrt{2N_c}}(2y-1).
\end{aligned} \tag{16}$$

The values of the Gegenbauer moments and decay constants for ϕ meson are taken as [69,70]

$$a_1^\parallel = a_1^\perp = 0, \qquad a_2^\parallel = 0.18 \pm 0.08, \qquad a_2^\perp = 0.14 \pm 0.07, \qquad f_\phi = (215 \pm 5)\ \text{MeV}, \qquad f_\phi^T = (186 \pm 9)\ \text{MeV}. \tag{17}$$

C. Invariant amplitudes and helicity amplitudes

The decay amplitude for $\frac{1}{2}^+ \to \frac{1}{2}^+ + 1^-$ type can be expanded with the Dirac spinors and polarization vector as [23,24],

$$\mathcal{M}^L = \bar{\Lambda}(p')\epsilon_L^{\mu*}\left[A_1^L\gamma_\mu\gamma_5 + A_2^L\frac{p'_\mu}{M}\gamma_5 + B_1^L\gamma_\mu + B_2^L\frac{p'_\mu}{M}\right]\Lambda_b(p),$$
$$\mathcal{M}^T = \bar{\Lambda}(p')\epsilon_T^{\mu*}[A_1^T\gamma_\mu\gamma_5 + B_1^T\gamma_\mu]\Lambda_b(p), \tag{18}$$

where we split the amplitude into the longitudinal and transverse pieces according to the vector meson polarizations [51]. Above we have included explicit factors of M so that $A(B)_2^L$ have the same dimensions as $A(B)_1^L$. The terms A and B denote the parity-violating and parity-conserving amplitudes, respectively. Their general factorization formula in PQCD can symbolically be written as

$$A(B) = \frac{f_{\Lambda_b}\pi^2 G_F}{18\sqrt{3}}\sum_{R_{ij}}\int[\mathcal{D}x][\mathcal{D}b]_{R_{ij}}\alpha_s^2(t_{R_{ij}})\Omega_{R_{ij}}(b,b',b_q) \times e^{-S_{R_{ij}}}\sum_{\sigma=LL,LR,SP} a_{R_{ij}}^\sigma H_{R_{ij}}^\sigma(x,x',y), \tag{19}$$

where the summation extends over all possible diagrams R_{ij}. $a_{R_{ij}}^\sigma$ denotes the product of the CKM matrix elements and the Wilson coefficients, and the labels $\sigma = LL$, LR, and SP refer to the contributions from $(V-A)(V-A)$, $(V-A)(V+A)$, and $(S-P)(S+P)$ operators, respectively. Here b, b' and b_q are the conjugate variables to k_T, k'_T and q_T, respectively. $H_{R_{ij}}^\sigma$ is the numerator of the hard amplitude depending on the spin structure of final state. $\Omega_{R_{ij}}$ is the Fourier transformation of the denominator of the hard amplitude from the k_T space to its conjugate b space. The integration measure of the momentum fractions are defined as

$$[\mathcal{D}x] = [dx_1dx_2dx_3\delta(1-x_1-x_2-x_3)] \times [dx'_1dx'_2dx'_3\delta(1-x'_1-x'_2-x'_3)]dy, \tag{20}$$

where the δ functions enforce momentum conservation. The hard scale t for each diagram is chosen as the maximal virtuality of internal particles including the factorization scales in a hard amplitude:

$$t_{R_{ij}} = \max\left(\sqrt{|t_A|}, \sqrt{|t_B|}, \sqrt{|t_C|}, \sqrt{|t_D|}, w, w', w_q\right), \tag{21}$$

where the expressions of $t_{A,B,C,D}$ will be listed in the Appendix. The factorization scales w, w', and w_q are defined by

$$w^{(\prime)} = \min\left(\frac{1}{b_1^{(\prime)}}, \frac{1}{b_2^{(\prime)}}, \frac{1}{b_3^{(\prime)}}\right), \qquad w_q = \frac{1}{b_q}, \tag{22}$$

with the variables

$$b_1^{(\prime)} = |b_2^{(\prime)} - b_3^{(\prime)}|, \tag{23}$$

and the other $b_l^{(\prime)}$ defined by permutation. The explicit forms of the Sudakov factors $S_{R_{ij}}$ can be found in [51]. Those quantities associated with specific diagram, such as $H_{R_{ij}}$, $a_{R_{ij}}$, $[\mathcal{D}b]_{R_{ij}}$, and $t_{R_{ij}}$, are collected in the Appendix.

It is convenient to apply the helicity amplitudes $H_{\lambda_\Lambda\lambda_\phi}$ for expressing various observable quantities in the decays, where λ_Λ and λ_ϕ are the respective helicities of Λ and ϕ with the possible values $\lambda_\Lambda = \pm 1/2$ and $\lambda_\phi = 0, \pm 1$. The helicity of the Λ_b baryon λ_{Λ_b} is related by $\lambda_{\Lambda_b} = \lambda_\Lambda - \lambda_\phi$ [23]. Angular momentum conservation allows four independent helicity amplitudes to contribute, including two transverse polarizations $H_{\pm\frac{1}{2}\pm 1}$ and two longitudinal ones $H_{\pm\frac{1}{2}0}$, which can be expressed in terms of the invariant amplitudes A and B as [23,24]

$$H_{\frac{1}{2}1} = -\left(\sqrt{Q_+}A_1^T + \sqrt{Q_-}B_1^T\right),$$
$$H_{-\frac{1}{2}-1} = \sqrt{Q_+}A_1^T - \sqrt{Q_-}B_1^T,$$
$$H_{\frac{1}{2}0} = \frac{1}{\sqrt{2}m_\phi}\left[\sqrt{Q_+}(M-m_\Lambda)A_1^L - \sqrt{Q_-}P_cA_2^L + \sqrt{Q_-}(M+m_\Lambda)B_1^L + \sqrt{Q_+}P_cB_2^L\right],$$
$$H_{-\frac{1}{2}0} = \frac{1}{\sqrt{2}m_\phi}\left[-\sqrt{Q_+}(M-m_\Lambda)A_1^L + \sqrt{Q_-}P_cA_2^L + \sqrt{Q_-}(M+m_\Lambda)B_1^L + \sqrt{Q_+}P_cB_2^L\right], \tag{24}$$

with $Q_\pm = (M \pm m_\Lambda)^2 - m_\phi^2$. $P_c = \sqrt{Q_+Q_-}/(2M)$ is the Λ momentum in the center of Λ_b mass frame.

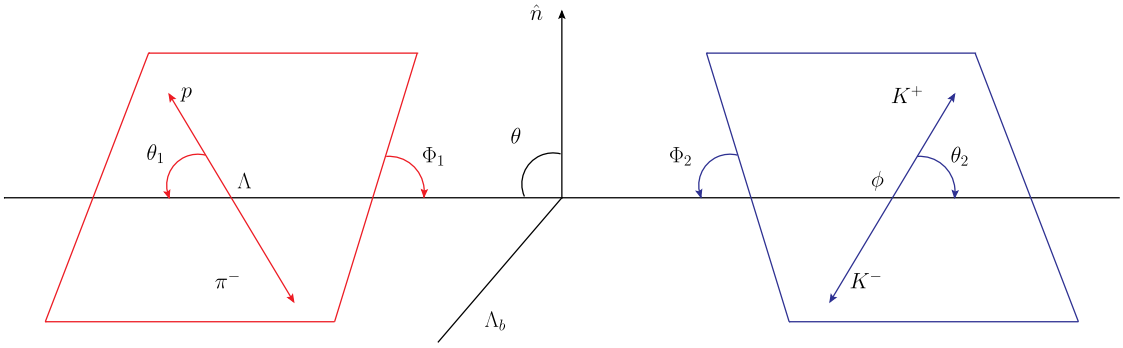

FIG. 4. Decay angles for the $\Lambda_b \to \Lambda(\to p\pi^-)\phi(\to K^+K^-)$ decay, where $\hat{n}$ is the normal unit-vector to the Λ_b production plane. θ is the polar angle of the Λ momentum with respect to $\hat{n}$ in the Λ_b rest-frame. The angles θ_1 and Φ_1 are respectively the polar and azimuthal angles of the proton momentum in the Λ rest frame while θ_2 and Φ_2 are those of K^+ in the ϕ rest frame.

The two-body decay branching ratio reads

$$\mathcal{B} = \frac{P_c \tau_{\Lambda_b}}{8\pi M^2} H_N, \tag{25}$$

where the sum of the magnitude squared of the helicity amplitudes H_N is denoted by

$$H_N = |H_{\frac{1}{2}1}|^2 + |H_{-\frac{1}{2}-1}|^2 + |H_{\frac{1}{2}0}|^2 + |H_{-\frac{1}{2}0}|^2. \tag{26}$$

D. Angular distributions and triple product asymmetries

Many asymmetry observables can be extracted from the angular distributions for the cascade decay $\Lambda_b \to \Lambda(\to p\pi^-)\phi(\to K^+K^-)$, which can be parametrized with three polar angles θ, θ_1, and θ_2 and two azimuthal angles Φ_1 and Φ_2 as illustrated in Fig. 4. The fivefold angular distribution is written as [11]

$$\frac{1}{\Gamma}\frac{d^5\Gamma}{d\Omega} = N \sum_{\lambda,\lambda'=\pm\frac{1}{2}} \left(\frac{1}{2} + \lambda P_b\right) \left| \sum_{\lambda_\Lambda,\lambda_\phi} A_{\lambda'} H_{\lambda_\Lambda,\lambda_\phi} d^{\frac{1}{2}}_{\lambda',\lambda_\Lambda-\lambda_\phi} \times (\theta) d^{\frac{1}{2}}_{\lambda_\Lambda,\lambda}(\theta_1) d^{1}_{\lambda_\phi,0}(\theta_2) e^{i(\lambda_\Lambda\phi_1+\lambda_\phi\phi_2)} \right|^2, \tag{27}$$

with $d\Omega = d\cos\theta d\cos\theta_1 d\cos\theta_2 d\Phi_1 d\Phi_2$. The first angle, θ, is the polar angle of the Λ momentum in the Λ_b rest-frame with respect to the normal direction of the Λ_b production plane. The two sets of solid angles (θ_1, Φ_1) and (θ_2, Φ_2) describe the decays of the Λ baryon and the ϕ meson in their respective rest-frame. $d^j_{mm'}$ is the Wigner-d function, which can be expanded into a sequence of trigonometric functions. P_b describes the polarization of Λ_b. $|A_{\lambda'}|^2 = (\frac{1}{2} + \lambda'\alpha_\Lambda)$ with α_Λ the up-down asymmetry parameters for $\Lambda \to p\pi^-$ [71]. N is an overall normalization factor such that the integration of Eq. (27) over $d\Omega$ is equal to one.

Similar to the case of B meson decays [72,73], a TPA A_T represents an asymmetry between the decay rates Γ with positive and negative values of TP,

$$A_T \equiv \frac{\Gamma(TP>0) - \Gamma(TP<0)}{\Gamma(TP>0) + \Gamma(TP<0)}, \tag{28}$$

where TP denotes a scalar triple product, which is odd under the time reversal transformation (T), and thus constitutes a potential signal of CP violation assuming CPT invariance. Choosing the appropriate TP, one can construct the asymmetries as follows [19]

$$A_T^1 = \frac{\Gamma(\cos\theta_2 \sin(\Phi_1+\Phi_2)>0) - \Gamma(\cos\theta_2 \sin(\Phi_1+\Phi_2)<0)}{\Gamma(\cos\theta_2 \sin(\Phi_1+\Phi_2)>0) + \Gamma(\cos\theta_2 \sin(\Phi_1+\Phi_2)<0)} = -\frac{\alpha_\Lambda}{\sqrt{2}} \frac{\mathrm{Im}[H_{\frac{1}{2}0} H^*_{-\frac{1}{2}-1} + H_{-\frac{1}{2}0} H^*_{\frac{1}{2}1}]}{H_N},$$

$$A_T^2 = \frac{\Gamma(\cos\theta_2 \sin\Phi_2>0) - \Gamma(\cos\theta_2 \sin\Phi_2<0)}{\Gamma(\cos\theta_2 \sin\Phi_2>0) + \Gamma(\cos\theta_2 \sin\Phi_2<0)} = -\frac{P_b}{\sqrt{2}} \frac{\mathrm{Im}[H_{-\frac{1}{2}-1} H^*_{-\frac{1}{2}0} + H_{\frac{1}{2}1} H^*_{\frac{1}{2}0}]}{H_N},$$

$$A_T^3 = \frac{\Gamma(\cos\theta\cos\theta_2 \sin(\Phi_1+\Phi_2)>0) - \Gamma(\cos\theta\cos\theta_2 \sin(\Phi_1+\Phi_2)<0)}{\Gamma(\cos\theta\cos\theta_2 \sin(\Phi_1+\Phi_2)>0) + \Gamma(\cos\theta\cos\theta_2 \sin(\Phi_1+\Phi_2)<0)} = \frac{P_b\alpha_\Lambda}{2\sqrt{2}} \frac{\mathrm{Im}[H_{-\frac{1}{2}-1} H^*_{\frac{1}{2}0} - H_{\frac{1}{2}1} H^*_{-\frac{1}{2}0}]}{H_N},$$

$$A_T^4 = \frac{\Gamma(\cos\theta_1\cos\theta_2 \sin\Phi_2>0) - \Gamma(\cos\theta_1\cos\theta_2 \sin\Phi_2<0)}{\Gamma(\cos\theta_1\cos\theta_2 \sin\Phi_2>0) + \Gamma(\cos\theta_1\cos\theta_2 \sin\Phi_2<0)} = \frac{P_b\alpha_\Lambda}{2\sqrt{2}} \frac{\mathrm{Im}[H_{-\frac{1}{2}-1} H^*_{-\frac{1}{2}0} - H_{\frac{1}{2}1} H^*_{\frac{1}{2}0}]}{H_N},$$

$$A_T^5 = \frac{\Gamma(\sin\Phi_1 > 0) - \Gamma(\sin\Phi_1 < 0)}{\Gamma(\sin\Phi_1 > 0) + \Gamma(\sin\Phi_1 < 0)} = -\frac{P_b \pi \alpha_\Lambda}{4} \frac{\mathrm{Im}[H_{-\frac{1}{2}0} H^*_{\frac{1}{2}0}]}{H_N},$$
$$A_T^6 = \frac{\Gamma(\sin(\Phi_1 + 2\Phi_2) > 0) - \Gamma(\sin(\Phi_1 + 2\Phi_2) < 0)}{\Gamma(\sin(\Phi_1 + 2\Phi_2) > 0) + \Gamma(\sin(\Phi_1 + 2\Phi_2) < 0)} = -\frac{P_b \pi \alpha_\Lambda}{4} \frac{\mathrm{Im}[H_{\frac{1}{2}1} H^*_{-\frac{1}{2}-1}]}{H_N}. \quad (29)$$

Then the true asymmetries are defined as [12,18]

$$A_T^i(\mathrm{true}) = \frac{A_T^i - \bar{A}_T^i}{2}, \quad (30)$$

where $\bar{A}_T^i$ with $i = 1$–6 are the corresponding quantities for the charge-conjugate process. A significant deviation from zero in these observables would indicate CP violation. Note that the above six asymmetries have the same forms as those in Ref. [11], apart from the additional multiplicative factors derived from the integral of the decay angles. Changing the sine of the azimuthal angle in above TP to cosine, we can obtain six new asymmetries, which are proportional to the real part of bilinear combinations of the helicity amplitudes. The corresponding expressions can be obtained from Eq. (29) with the replacement of $\mathrm{Im} \to \mathrm{Re}$. Similarly, combining the quantities for the corresponding CP-conjugate process, they have the form of $\mathrm{Re}[H' H^* - \bar{H}' \bar{H}^*]$, which is characteristic of direct CP asymmetry.

Integrating Eq. (27) over the two azimuthal angles Φ_1 and Φ_2, the angular distribution is reduced to eight terms as shown in [74] (see Table 2), which can be written in terms of the following three independent angular observables

$$\alpha_b = -|\hat{H}_{\frac{1}{2}1}|^2 + |\hat{H}_{-\frac{1}{2}-1}|^2 + |\hat{H}_{\frac{1}{2}0}|^2 - |\hat{H}_{-\frac{1}{2}0}|^2,$$
$$r_0 = |\hat{H}_{\frac{1}{2}0}|^2 + |\hat{H}_{-\frac{1}{2}0}|^2,$$
$$r_1 = |\hat{H}_{\frac{1}{2}0}|^2 - |\hat{H}_{-\frac{1}{2}0}|^2, \quad (31)$$

with $|\hat{H}_{\lambda_\Lambda \lambda_\phi}|^2 = |H_{\lambda_\Lambda \lambda_\phi}|^2 / H_N$. The asymmetry parameter α_b characterizes parity nonconservation in a weak decay of Λ_b. r_0 and r_1 are the longitudinal unpolarized and polarized parameters, respectively.

Further integrating (θ, θ_2) and (θ, θ_1), respectively, one can extract two more interesting asymmetries

$$\alpha_{\lambda_\Lambda} = |\hat{H}_{\frac{1}{2}0}|^2 + |\hat{H}_{\frac{1}{2}1}|^2 - |\hat{H}_{-\frac{1}{2}-1}|^2 - |\hat{H}_{-\frac{1}{2}0}|^2,$$
$$\alpha_{\lambda_\phi} = |\hat{H}_{\frac{1}{2}0}|^2 + |\hat{H}_{-\frac{1}{2}0}|^2 - |\hat{H}_{\frac{1}{2}1}|^2 - |\hat{H}_{-\frac{1}{2}-1}|^2, \quad (32)$$

where the former describes the polarization of Λ baryon, and the latter represents the asymmetry between the longitudinal and transverse polarizations of ϕ meson. We see that α_{λ_Λ} and α_{λ_ϕ} are odd and even under parity transformation, respectively.

III. NUMERICAL RESULTS

Numerical results on the invariant and helicity amplitudes, branching ratio, angular observables, direct CP violation, and TPAs will be presented in this section. In our numerical study, the values of relevant masses (GeV), lifetimes (ps), and the Wolfenstein parameters for the CKM matrix are taken from the latest experimental values [7]:

$$M = 5.6196, \quad m_\Lambda = 1.116, \quad m_b = 4.8, \quad m_\phi = 1.019,$$
$$\tau = 1.464, \quad \lambda = 0.22650, \quad A = 0.790, \quad \bar{\rho} = 0.141, \quad \bar{\eta} = 0.357. \quad (33)$$

Other nonperturbative parameters appearing in the hadron LCDAs have been specified in the preceding section.

As stressed before, all the five topologies can be evaluated systematically in PQCD. It is interesting to compare the relative strengths among these topologies, whose results are shown separately in Table I. The labels P, $PE(PB)$, and $E(B)$ corresponds to the contributions from the penguin emission, penguin exchange, and W exchange, respectively, and the last column is their sum. It is found that the decay amplitudes are governed by the penguin emission P and penguin exchange diagrams PE, which contribute at the same order of magnitude, while the W exchange ones suffer from severe CKM suppression and are smaller by one or two orders of magnitude. The contributions from B and PB-type exchange diagrams are predicted to be vanishingly small.

In order to understand the mechanism responsible for the large contribution from the PE diagrams, one has to compare the relative contributions from various components in the LCDAs. In this study we take into account the contributions from the Λ_b baryon LCDAs up to twist 4 and the ϕ meson LCDAs up to twist 3, while the Λ one is

TABLE I. Contributions from the various topologies to the invariant amplitudes (10^{-10}) for $\Lambda_b \to \Lambda\phi$ decay. The labels P, $PE(PB)$, and $E(B)$ corresponds to the contributions from the penguin emission, penguin exchange, and the W exchange diagrams, respectively, and the last column is their sum. Only central values are presented here.

Amplitude	P	PE	E	PB	B	Total
A_1^L	$-0.59 - i3.90$	$4.24 - i10.82$	$1.14 + i0.71$	$0.39 + i0.02$	$-0.02 + i0.05$	$5.16 - i13.94$
B_1^L	$-1.69 + i4.05$	$-3.86 + i12.20$	$-1.46 - i0.83$	$-0.56 + i0.00$	$0.01 - i0.07$	$-7.55 + i15.36$
A_2^L	$0.43 - i36.09$	$9.45 - i25.39$	$2.66 + i1.65$	$1.47 + i0.02$	$-0.04 + i0.14$	$13.97 - i59.67$
B_2^L	$2.75 - i15.10$	$7.92 - i19.70$	$2.59 + i1.28$	$0.64 + i0.01$	$-0.03 + i0.13$	$13.87 - i33.39$
A_1^T	$-0.53 - i2.54$	$2.22 - i4.70$	$0.64 + i0.59$	$0.14 - i0.11$	$0.00 + i0.03$	$2.47 - i6.73$
B_1^T	$-1.99 + i2.73$	$-2.00 + i5.45$	$-1.08 - i0.69$	$-0.20 + i0.21$	$0.00 - i0.04$	$-5.26 + i7.65$

TABLE II. The contributions from Φ^V, Φ^A, and Φ^T in the Λ baryon LCDAs to the invariant amplitudes.

Amplitude	Φ^V	Φ^A	Φ^T
A_1^L	$1.3 \times 10^{-13} + i7.5 \times 10^{-11}$	$5.7 \times 10^{-10} - i1.2 \times 10^{-9}$	$-5.0 \times 10^{-11} - i2.8 \times 10^{-10}$
B_1^L	$4.5 \times 10^{-11} - i1.3 \times 10^{-10}$	$-9.2 \times 10^{-10} + i1.3 \times 10^{-9}$	$1.2 \times 10^{-10} + i3.7 \times 10^{-10}$
A_2^L	$-2.5 \times 10^{-10} + i6.4 \times 10^{-11}$	$1.3 \times 10^{-9} - i4.3 \times 10^{-9}$	$4.0 \times 10^{-10} - i1.8 \times 10^{-9}$
B_2^L	$9.0 \times 10^{-11} + i9.4 \times 10^{-11}$	$1.5 \times 10^{-9} - i3.5 \times 10^{-9}$	$-2.1 \times 10^{-10} + i3.4 \times 10^{-11}$
A_1^T	$-2.8 \times 10^{-11} + i1.0 \times 10^{-11}$	$2.9 \times 10^{-10} - i5.0 \times 10^{-10}$	$-1.3 \times 10^{-11} - i1.8 \times 10^{-10}$
B_1^T	$1.2 \times 10^{-10} + i2.9 \times 10^{-13}$	$-6.7 \times 10^{-10} + i5.4 \times 10^{-10}$	$2.1 \times 10^{-11} + i2.3 \times 10^{-10}$

restricted to the leading-twist accuracy. We first compare in Table II the values of the invariant amplitudes from three components of the leading-twist LCDAs of Λ baryon. It is observed that the mainly contributions come from the component Φ^A as a consequence of the symmetry relations in Eq. (12). Conversely, contributions from the components Φ^V and Φ^T are relative small due to the antisymmetry under the interchange of x and $1-x$. In particular, the contribution of Φ^V is further suppressed by the small coefficients of the terms $x_2^2 - x_3^2$ and $x_2 - x_3$ in Eq. (12). Similar feature has also been observed in previous PQCD calculations on the $\Lambda_b \to \Lambda J/\psi$ mode [43,51]. Contributions from twist-2 and twist-3 LCDAs of ϕ meson are also displayed separately in Table III. It can be shown that their contributions are comparable. The important twist-3 meson LCDAs contributions were also observed in the penguin-dominated B meson decay, such as $B_s \to \phi\phi$ [75].

Given this situation, it is expected that the dominant contribution to the invariant amplitudes comes from the combination of Φ^A and twist-2 LCDAs of Λ_b, such as the $\Phi^A\Psi_2$ term. Note that the invariant amplitudes involve different sets of Λ_b baryon LCDAs through different Feynman diagrams. In the following analysis we take diagrams of $P_{c7,d6}$ and PE_{b3} as examples to illustrate, which dominate the P and PE-type amplitudes, respectively. As can be seen from Table XII that the dominant term $\Phi^A\Psi_2$ contributes to A_1, B_1 and A_2, B_2 through the nonfactorizable diagrams P_{d6} and P_{c7}, respectively. Thus the penguin emission decay amplitudes are governed by the twist-2 contributions. Nevertheless, for the penguin exchange diagram PE_{b3}, the twist-2 term vanish at the level of the theoretical accuracy in the current formalism. The leading contribution to PE_{b3} comes from the twist-4 term, $\Phi^A\Psi_4$. As stated in [49], the higher-twist effects are crucial

TABLE III. The values of invariant amplitude from twist-2 and twist-3 LCDAs of ϕ meson for $\Lambda_b \to \Lambda\phi$ decays.

Amplitude	twist-2	twist-3
A_1^L	$1.0 \times 10^{-10} - i2.0 \times 10^{-10}$	$4.1 \times 10^{-10} - i1.2 \times 10^{-9}$
B_1^L	$-3.9 \times 10^{-10} + i2.3 \times 10^{-10}$	$-3.7 \times 10^{-10} + i1.3 \times 10^{-9}$
A_2^L	$3.9 \times 10^{-10} - i3.5 \times 10^{-9}$	$1.0 \times 10^{-9} - i2.4 \times 10^{-9}$
B_2^L	$4.7 \times 10^{-10} - i9.9 \times 10^{-10}$	$9.2 \times 10^{-10} - i2.3 \times 10^{-9}$
A_1^T	$2.9 \times 10^{-10} - i5.0 \times 10^{-10}$	$-4.7 \times 10^{-11} - i1.8 \times 10^{-10}$
B_1^T	$-2.5 \times 10^{-10} + i5.7 \times 10^{-10}$	$-2.8 \times 10^{-10} + i2.0 \times 10^{-10}$

TABLE IV. The values of the invariant amplitudes from various twists of the Λ_b baryon LCDAs for P and PE diagrams.

Amplitude	Twist	P	PE
A_1^L	2	$6.0\times10^{-11}-i1.3\times10^{-10}$	$2.8\times10^{-11}+i6.5\times10^{-11}$
	3	$-1.0\times10^{-10}-i4.9\times10^{-11}$	$4.4\times10^{-11}-i1.6\times10^{-10}$
	4	$-1.7\times10^{-11}-i2.1\times10^{-10}$	$3.5\times10^{-10}-i9.9\times10^{-10}$
B_1^L	2	$-6.7\times10^{-11}+i1.3\times10^{-10}$	$-2.8\times10^{-11}-i9.0\times10^{-11}$
	3	$1.6\times10^{-10}-i3.0\times10^{-11}$	$5.3\times10^{-11}+i4.2\times10^{-10}$
	4	$-2.6\times10^{-10}+i3.0\times10^{-10}$	$-4.1\times10^{-10}+i8.9\times10^{-10}$
A_2^L	2	$2.5\times10^{-10}-i2.2\times10^{-9}$	$9.8\times10^{-11}+i2.2\times10^{-10}$
	3	$-7.1\times10^{-11}-i1.1\times10^{-9}$	$7.3\times10^{-11}-i8.5\times10^{-10}$
	4	$-1.3\times10^{-10}-i2.6\times10^{-10}$	$7.7\times10^{-10}-i1.9\times10^{-9}$
B_2^L	2	$1.8\times10^{-10}-i1.5\times10^{-9}$	$2.7\times10^{-11}+i1.1\times10^{-10}$
	3	$-2.7\times10^{-10}+i4.0\times10^{-10}$	$1.1\times10^{-10}-i3.9\times10^{-10}$
	4	$3.6\times10^{-10}-i4.4\times10^{-10}$	$6.5\times10^{-10}-i1.7\times10^{-9}$
A_1^T	2	$2.5\times10^{-11}-i5.9\times10^{-11}$	$-1.7\times10^{-11}+i2.9\times10^{-11}$
	3	$-1.0\times10^{-10}-i7.7\times10^{-12}$	$4.3\times10^{-11}-i1.6\times10^{-10}$
	4	$2.3\times10^{-11}-i1.9\times10^{-10}$	$2.0\times10^{-10}-i3.4\times10^{-10}$
B_1^T	2	$-3.3\times10^{-11}+i6.2\times10^{-11}$	$2.5\times10^{-11}-i4.6\times10^{-11}$
	3	$1.8\times10^{-10}+i2.0\times10^{-12}$	$2.3\times10^{-11}+i2.9\times10^{-10}$
	4	$-3.4\times10^{-10}+i2.1\times10^{-10}$	$-2.5\times10^{-10}+i3.0\times10^{-10}$

at the realistic scale of the b quark mass, and the contribution from twist-4 Λ_b baryon LCDAs could overcome the power suppression from $1/M$ with respect to the twist-2 one due to the enhancement from the endpoint region. It is not surprising that the twist-2 and twist-4 contributions are of the same order for a similar reason in this work. Therefore we can explain why the penguin exchange amplitudes are in fact at the same order as the penguin emission ones, which can be seen in the columns of P and PE of Table I.

Table IV indicates clearly that the higher-twist contributions significantly enhance the penguin exchange amplitudes. The picture of significant exchange topological contributions differs from the case of the color-allowed decays of $\Lambda_b\to\Lambda_c\pi,\Lambda_cK$ [50], in which the emission type amplitude is dominant and accounts for more than 90% of the total decay amplitudes. We should point out, however, that only the leading-twist LCDAs of the Λ_b baryon was considered in [50]. The hierarchy relationship may be modified to some extent if the higher-twist contributions are included, which is an intriguing topic for future research.

The factorizable amplitudes contribute only via the penguin emission diagrams, such as P_{a1-a5}, P_{b1-b5}, and $P_{e1,e2,f1,f2}$ as shown in Fig. 1, in which the $s\bar{s}$ of ϕ mesons are created by weak vertices. In Table V, we present the factorizable and nonfactorizable contributions in the decay amplitudes. It is observed that the nonfactorizable contributions dominate over the factorizable ones, which is similar to the cases of the decay of $\Lambda_b\to\Lambda J/\psi$ [43,51] and $\Lambda_b\to p\pi,pK$ [48].

By using the results of Table I, one can calculate the helicity amplitudes according to Eq. (24), whose numerical results are displayed in the Table VI. It is observed that the amplitudes are dominated by $H_{-\frac{1}{2}0}$ which occupies about 81% of the full contribution. It implies the negative-helicity component of the Λ baryon and longitudinally polarized ϕ meson in the final states are preferred. Contributions from the transverse polarizations of ϕ meson are rather small, which amounts to less than 10%. As pointed out in [76], the transverse amplitudes are suppressed relative to the longitudinal ones by a factor r_ϕ, which can also be seen from Eq. (24). This situation differs from the case of $\Lambda_b\to\Lambda J/\psi$ decays [51], where their contributions are comparable because the J/ψ is very heavy (three times as lager as the ϕ), and thus the suppression is not obvious. The domination of $H_{-\frac{1}{2}0}$ is consistent with the expectation from the heavy-quark limit and the left-handed nature of the

TABLE V. The values of the invariant amplitudes from the factorizable and nonfactorizable diagrams for $\Lambda_b\to\Lambda\phi$ decay.

Amplitude	Factorizable	Nonfactorizable
A_1^L	-1.5×10^{-11}	$5.3\times10^{-10}-i1.4\times10^{-9}$
B_1^L	-2.7×10^{-11}	$-7.3\times10^{-10}+i1.5\times10^{-9}$
A_2^L	-6.1×10^{-11}	$1.5\times10^{-9}-i6.0\times10^{-9}$
B_2^L	6.3×10^{-11}	$1.3\times10^{-9}-i3.3\times10^{-9}$
A_1^T	-1.5×10^{-11}	$2.6\times10^{-10}-i6.7\times10^{-10}$
B_1^T	-3.1×10^{-11}	$-5.0\times10^{-10}+i7.7\times10^{-10}$

TABLE VI. Helicity amplitudes and phases of $\Lambda_b \to \Lambda\phi$ decay. The last row corresponds to the magnitude squared of normalized helicity amplitudes.

$\lambda_\Lambda\lambda_\phi$	$\frac{1}{2}1$	$-\frac{1}{2}-1$	$\frac{1}{2}0$	$-\frac{1}{2}0$
$H_{\lambda_\Lambda\lambda_\phi}$	$6.6\times10^{-10}+i1.1\times10^{-9}$	$4.0\times10^{-9}-i7.9\times10^{-9}$	$8.6\times10^{-10}+i9.9\times10^{-9}$	$1.6\times10^{-9}-i2.8\times10^{-8}$
$\Phi_{\lambda_\Lambda\lambda_\phi}$	1.04	−1.10	1.48	−1.51
$\lvert\hat{H}_{\lambda_\Lambda\lambda_\phi}\rvert^2$	2.0×10^{-3}	8.3×10^{-2}	0.105	0.81

TABLE VII. Branching ratios and asymmetry parameters for the $\Lambda_b \to \Lambda\phi$ decay. The theoretical errors correspond to the uncertainties due to $\omega = 0.40 \pm 0.04$ GeV and the hard scale $t = (1.0 \pm 0.2)t$, respectively.

$\mathcal{B}$	α_b	α_{λ_Λ}	α_{λ_ϕ}	r_0	r_1
$6.9^{+1.9+1.8}_{-2.0-1.6}\times10^{-6}$	$-0.63^{+0.16+0.00}_{-0.01-0.03}$	$-0.79^{+0.12+0.00}_{-0.02-0.04}$	$0.83^{+0.03+0.01}_{-0.03-0.05}$	$0.91^{+0.01+0.01}_{-0.02-0.02}$	$-0.71^{+0.14+0.00}_{-0.01-0.02}$

weak interaction and the prediction in GFA [11]. As shown in [11], the four helicity amplitudes in the GFA share the same complex phase, which come from the common effective Wilson coefficients. However, in our calculation, the nonfactorizable contributions are the major source of the strong phases, and each helicity amplitude has a different phase as exhibited in Table V.

After obtaining the values of the helicity amplitudes, we can compute the branching ratio and various asymmetries through Eqs. (25), (31), and (32). The numerical results are collected in Table VII, where the first and second uncertainties arise from the shape parameter $\omega_0 = 0.40 \pm 0.04$ GeV in the Λ_b baryon LCDAs and hard scale t varying from $0.8t$ to $1.2t$, respectively. We draw the following observations:

(1) The PQCD prediction of the branching ratio involves a large uncertainty because of the sensitivity to the nonperturbative hadronic LCDAs, which are of limited accuracy due to our lack of understanding of QCD dynamics at low energies. Pinning down the uncertainties of LCDAs is an essential prescription to improve the accuracy of PQCD calculations. In contrast to the branching ratio, most of the asymmetry observables are insensitive to the nonperturbative QCD effects because the resulting uncertainties have been eliminated in the ratios, indicates they can serve as the ideal quantities to test the PQCD approach.

(2) The predicted branching ratio is slightly larger than the LHCb measured value $(5.18 \pm 1.29) \times 10^{-6}$ [5], where multiple uncertainties are added in quadrature. However, recent updates from the PDG on the web and the world average from the Heavy Flavor Averaging Group (HFLAV) give $(9.8 \pm 2.6) \times 10^{-6}$ and $(10.1^{+2.9}_{-2.5}) \times 10^{-6}$ [77], respectively. Both of the central values are larger than the LHCb data by a factor of two. We notice that in fact all these data come from the measurement of the relative branching fraction of $\Lambda_b \to \Lambda\phi$ to $B^0 \to K^0\phi$ by LHCb [5], and the discrepancies are mainly caused by using different values for the production rate ratio f_{Λ_b}/f_d with $f_{\Lambda_b}(f_d)$ being the fragmentation fractions of b quarks to $\Lambda_b(B^0)$.

(3) By comparison, the estimates based on GFA gives $\mathcal{B}(\Lambda_b \to \Lambda\phi) = (1.77^{+1.76}_{-1.71} \pm 0.24) \times 10^{-6}$ [9], which suffers large uncertainties from the nonfactorizable effects. With the number of colors setting as $N^{\rm eff} = 2$, the value can be enhanced to $(3.53 \pm 0.24) \times 10^{-6}$, which is still half of our prediction and apparently lower than the world averages. The result from the QCDF [8], yields $(6.33^{+0.60+1.57+0.83}_{-0.68-1.56-0.61}) \times 10^{-7}$, is below our number by roughly one order of magnitude. The smallness is ascribed to the important nonfactorizable effects, such as hard spectator interactions and power corrections, were not included in their calculations.

(4) The up-down asymmetry α_b is predicted to be $-0.63^{+0.16+0.00}_{-0.01-0.03}$ in PQCD, away from -1 because the considered process also receives sizeable contributions from the QCD penguin operators $O_{5,6,7,8}$ via the $V + A$ current. Our central value is somewhat larger than the QCDF calculation −0.8 presented in [8]. The asymmetry parameters of α_{λ_Λ} and α_{λ_ϕ} evaluated in GFA are −0.99 and 0.86 [11], respectively, which are comparable to our results in Table VII. The obtained predictions on the r_0 and r_1, received less theoretical and experimental attentions, can be compared in future.

We now discuss the TPAs in $\Lambda_b \to \Lambda\phi$ decay. From Eq. (29), one can see that two parameters α_Λ and P_b enter into the angular distribution and appear in the TPAs. For the former, we use the new experimental PDG average values $\alpha_\Lambda = 0.732 \pm 0.014$ and $\alpha_{\bar{\Lambda}} = -0.758 \pm 0.012$ [7], deduced from the measurements by the BES-III [71] and CLAS [78] Collaborations. The value of P_b is annoying because it depends on the production mechanism of the Λ_b. Here we assume that Λ_b baryons are produced

directly in the hadron collisions, where the longitudinal polarization is expected to vanish due to parity conservation in strong interactions [79]. The CP invariance between the Λ_b and $\bar{\Lambda}_b$ angular distributions implies the relation of $\bar{P}_b = -P_b$ can be used [80]. Experimentally, the polarization had been measured from the angular distributions of $\Lambda_b \to \Lambda J/\psi$ decay by the LHCb [79], CMS [80] and ATLAS [81] experiments, which have yielded a value consistent with zero, though polarization of 10% is possible given statistical uncertainties [74]. Theoretically, it has been suggested that the value of P_b would reach up to the (10–20)% level [14,82]. In the following analysis, we take $P_b = 0.1$ as a rough numerical estimates.

The calculated TPAs in GFA must be zero [11] since their helicity amplitudes share the same complex phase as mentioned above. In contrast, in PQCD regime, the helicity amplitudes always have different strong phases, which mainly originate from the nonfactorizable diagrams as shown in Table V. This will lead to nonzero TPAs, which are summarized in Table VIII. As expected the PQCD results on these asymmetries come out to be quite small, range from 10^{-4} to 10^{-2}. A_T^1 do not involve the polarization of the initial state and could be measured in the unpolarized angular distribution. Its relative large value of order 10^{-2} makes it is the best candidate to look for in experimental searches. The small values of A_T^3 and A_T^4 are mainly attributed by a substantial cancellation of the two component as can be seen in Eq. (29). The difference between A_T^2 and A_T^4 is ascribed to the distinct combinations of $H_{-\frac{1}{2}-1}H^*_{-\frac{1}{2}0}$ and $H_{\frac{1}{2}1}H^*_{\frac{1}{2}0}$ in Eq. (29). The smallness of A_T^6 can be traced to the transverse polarization components suffer the power suppression as explained above. In addition, the W exchange amplitudes associated with the CKM matrix elements $V_{ub}V^*_{us}$ provide the weak phase, which interfere with the penguin amplitudes to produce nonvanishing true TPAs as given in the last column of Table VIII. As noted previously, W exchange contributions are highly CKM suppressed relative to the penguin ones, most the true TPAs are estimated to be less than $\mathcal{O}(1\%)$ in magnitude, compatible with the absence of CP violation.

TABLE VIII. PQCD predictions for the TPAs with $P_b = 0.1$. The sources of the theoretical errors are the same as in Table VII but added in quadrature.

	A_T^i	$\bar{A}_T^i$	A_T^i(true)
i = 1	$-1.4^{+4.5}_{-0.1} \times 10^{-2}$	$1.3^{+2.0}_{-3.7} \times 10^{-2}$	$-1.4^{+4.1}_{-1.1} \times 10^{-2}$
i = 2	$-6.9^{+0.0}_{-0.4} \times 10^{-3}$	$-3.5^{+2.8}_{-3.6} \times 10^{-3}$	$-1.7^{+1.8}_{-1.6} \times 10^{-3}$
i = 3	$-1.8^{+2.2}_{-0.6} \times 10^{-3}$	$-5.7^{+0.0}_{-1.7} \times 10^{-4}$	$-0.6^{+1.2}_{-0.3} \times 10^{-3}$
i = 4	$2.8^{+2.3}_{-0.0} \times 10^{-3}$	$1.8^{+2.0}_{-1.6} \times 10^{-3}$	$0.5^{+2.0}_{-1.0} \times 10^{-3}$
i = 5	$2.4^{+0.0}_{-1.8} \times 10^{-3}$	$-3.6^{+1.2}_{-0.2} \times 10^{-3}$	$3.0^{+0.1}_{-1.5} \times 10^{-3}$
i = 6	$-5.9^{+0.0}_{-0.4} \times 10^{-4}$	$-5.5^{+0.0}_{-0.1} \times 10^{-4}$	$-0.2^{+0.1}_{-0.2} \times 10^{-4}$

We therefore conclude that any measurement of a sizeable TPAs in the decay is an unequivocal signal of new physics.

The partial angular analysis of the considered process has been studied by LHCb [5], in which four asymmetries are measured to be consistent with zero. Note that these asymmetries are defined by the so-called special angles [17], which are explicitly given in Ref. [19]. As stated in [19], such angular asymmetries give access to terms proportional to the off-diagonal elements of the Λ_b polarization density matrix, which are absent in the current case since the Λ_b is assumed to be produced by the strong interaction which preserves parity. Therefore all the four asymmetries vanish in our calculations.

Finally, we predict the direct CP asymmetry of the $\Lambda_b \to \Lambda\phi$ decay, which is defined by

$$A_{CP} = \frac{\Gamma(\Lambda_b \to \Lambda\phi) - \Gamma(\bar{\Lambda}_b \to \bar{\Lambda}\phi)}{\Gamma(\Lambda_b \to \Lambda\phi) + \Gamma(\bar{\Lambda}_b \to \bar{\Lambda}\phi)}, \tag{34}$$

where the overline denotes the antiparticles. It is known that at least two amplitudes with nontrivial relative strong and weak phases are required to produce a nonvanishing direct CP violation. As already remarked above, the tree amplitudes contribute via the W exchange diagrams, while the penguin ones exist in both penguin emission and exchange diagrams. The direct CP asymmetry arises from the interference between the tree and penguin amplitudes. Since the tree-level W exchange contribution is suppressed by the CKM matrix elements $|V_{ub}V^*_{us}/V_{tb}V^*_{ts}| \sim 0.02$ compared with the penguin ones, the resulting direct CP asymmetry would be very small with the value of $-1.0^{+1.0}_{-1.5}\%$, where the sources of the theoretical errors are the same as in Table VII but added in quadrature. The corresponding value from QCDF and GFA are $1.6^{+0.4}_{-0.3}\%$ [8] and $1.4^{+0.7}_{-0.1}\%$ [10], respectively. Our central value agrees with theirs in magnitude but differs in sign. These results can be checked by future experiments.

IV. CONCLUSION

The weak decay of the bottom baryon provides useful information about the strong interaction and serves as an important probe for testing various theoretical approaches. Because baryons are three-quark systems in the conventional quark model, their weak decays contain a large number of topological diagrams, making QCD dynamics involved in the hadronic matrix element extremely complicated. Nonfactorizable contributions, in particular the exchange topological contributions, are more difficult to evaluate from first principles. The perturbative QCD approach is a powerful tool to analyze the heavy baryon decays, in which both the emission and exchange topologies can be evaluated systematically. In this work, we have carried out a systematic study on the penguin-dominant $\Lambda_b \to \Lambda\phi$ decay, whose branching ratio was predicted to be

much small in previous literature with only the emission topological contributions being taken into account. Since the PQCD calculations of the baryon decay start at two order of α_s, $\Lambda_b \to \Lambda\phi$ proceeds simultaneously through the charged current $b \to u$ transition and neutral-current $b \to s$ transition. The former corresponds to the tree diagrams contribution resulting from the W exchange diagrams, while the latter belongs to the penguin contributions, which could be further cataloged into penguin emission and penguin exchange ones. All the possible Feynman diagrams can be classified into five topological types, namely P, PE, E, B, and PB, respectively. It is observed that the decay amplitudes are dominated by the P and PE-type diagrams, while contributions from the W exchange ones suffer from severe CKM suppression. Furthermore, the contributions from B and PB-type exchange diagrams are predicted to be vanishingly small.

After the standard PQCD calculations, we obtain the factorization formulas for the invariant amplitudes, which can be transformed into the helicity amplitudes for more convenient analysis of the asymmetry parameters in the angular distribution. Angular momentum conservation allows four complex helicity amplitudes to contribute in the decay under scrutiny. Differing from the calculations in GFA, where the helicity amplitudes share the same complex phase, the strong phase in our approach is primarily derived from nonfactorizable contribution that is special to each helicity amplitude. Both the moduli and phases of these helicity amplitudes could be predicted in PQCD, which allows one to compute the nonzero triple product asymmetries originating from the interference among various helicity amplitudes. We found that the negative helicity component of the Λ baryon and longitudinally polarized ϕ meson in the final states are preferred. This pattern observed is in line with the expectation from the heavy-quark limit and the left-handed nature of the weak interaction and the GFA prediction.

Our prediction of $6.9^{+1.9+1.8}_{-2.0-1.6} \times 10^{-6}$ for its branching ratio is comparable with the world averages from PDG and HFLAV, whereas the theoretical estimates based on GFA and QCDF have shown sizeable deviations. The representative theoretical uncertainties from the nonperturbative parameters in Λ_b LCDAs and the hard scale were taken into account, which can reach 30% in magnitude. However, most of the asymmetry observables are less sensitive to the variations of hadronic parameters owing to the cancellations of uncertainties in the ratios. The direct CP asymmetry is estimated to reach the percent level, which is consistent with the results from GFA and QCDF. These obtained asymmetries can be confronted with the future data.

We give the first theoretical estimates of the triple product asymmetries in the polarized decay distributions, which can be expressed by the imaginary part of bilinear combinations of the helicity amplitudes, the asymmetry parameter α_Λ related to $\Lambda \to p\pi$ decay, and the Λ_b polarization fraction P_b. For numerical estimations, we have used the value of α_Λ as given in PDG and set $P_b = 0.1$. The predicted values of TPAs for $\Lambda_b \to \Lambda\phi$ and their CP conjugate counterparts are in the range from 10^{-4} to 10^{-2}. Among these asymmetries, only A_T^1 is independent of P_b and has a largest value at 10^{-2} level, which can be measured with the unpolarized angular distribution. Combining the TPAs in Λ_b and $\bar{\Lambda}_b$ decays, we obtain the PQCD predictions on the true TPAs, which are tiny, of order 10^{-2} or even lower. The smallness of these true asymmetries are compatible with CP conservation. Hence, the measurement of a large true TPAs would be a clean indication of new CP violation mechanism beyond the standard model.

ACKNOWLEDGMENTS

We would like to acknowledge Yue-Long Shen and Fu-Sheng Yu for helpful discussions. This work is supported by National Natural Science Foundation of China under Grants No. 12075086 and No. 11605060 and the Natural Science Foundation of Hebei Province under Grants No. A2021209002 and No. A2019209449.

APPENDIX: FACTORIZATION FORMULAS

Following the conventions in Ref. [50], we provide some details about the factorization formulas in Eq. (19). The combinations of the Wilson coefficients $a^\sigma_{R_{ij}}$ are collected in Table IX. The virtualities of the internal propagators $t_{A,B,C,D}$ and the expressions of $[\mathcal{D}b]$ and $\Omega_{R_{ij}}$ for the exchange diagrams are gathered in Tables X and XI, respectively, where the auxiliary functions $h_{1,2,3}$ and the Bessel function K_0 can be found in [50]. The corresponding forms for the P-type diagrams can be found in Refs. [50,51] and shall not be repeated here.

In Table XII, we give the expressions of $H^{LL,LR,SP}_{R_{ij}}$ in the invariant amplitudes $A_1^{T,L}$ and A_2^L for some main contributing Feynman diagrams, while the remaining ones can be derived in a similar way. The corresponding formulas for those B terms can be obtained by the following replacement:

$$B_1^{T,L} = A_1^{T,L}|_{r_\phi \to -r_\phi, r_\Lambda \to -r_\Lambda, \Phi^T \to -\Phi^T},$$
$$B_2^L = A_2^L|_{r_\phi \to -r_\phi, r_\Lambda \to -r_\Lambda, \Phi^V \to -\Phi^V, \Phi^A \to -\Phi^A}. \quad \text{(A1)}$$

TABLE IX. The expressions of a^{LL}, a^{LR} and a^{SP} in Eq. (19) for the exchange topological diagrams.

R_{ij}	a^{LL}	a^{LR}	a^{SP}
$P_{a1,a2,a3,a5,b1,b2,b4}$	$V_{tb}V_{ts}^*[\frac{4}{3}(C_3+C_4)-\frac{2}{3}(C_9+C_{10})]$	$V_{tb}V_{ts}^*[C_6+\frac{1}{3}C_5-\frac{1}{2}C_8-\frac{1}{6}C_7]$	$V_{tb}V_{ts}^*[C_5+\frac{1}{3}C_6-\frac{1}{2}C_7-\frac{1}{6}C_8]$
$P_{a6,a7,b6,b7,c1,c2,d1,d2}$	$V_{tb}V_{ts}^*[\frac{1}{3}(C_3+C_4)-\frac{1}{6}(C_9+C_{10})]$	$V_{tb}V_{ts}^*[\frac{1}{3}C_5-\frac{1}{6}C_7]$	$V_{tb}V_{ts}^*[\frac{1}{3}C_6-\frac{1}{6}C_8]$
$P_{c5,c7,d6}$	$V_{tb}V_{ts}^*[\frac{1}{12}(C_3+C_4)-\frac{1}{24}(C_9+C_{10})]$	$V_{tb}V_{ts}^*[\frac{1}{3}C_5-\frac{1}{4}C_6-\frac{1}{6}C_7+\frac{1}{8}C_8]$	$V_{tb}V_{ts}^*[\frac{1}{3}C_6-\frac{1}{4}C_5-\frac{1}{6}C_8+\frac{1}{8}C_7]$
$PE_{a1-a7,e1-e4,f4}$	$V_{tb}V_{ts}^*[\frac{2}{3}(C_3-C_4)+\frac{1}{6}(C_9-C_{10})]$	$V_{tb}V_{ts}^*[\frac{2}{3}(C_5-C_6)+\frac{1}{6}(C_7-C_8)]$	⋯
$PE_{b1,b3,b5,b7}$	$\frac{1}{3}V_{tb}V_{ts}^*[2C_3+4C_4+\frac{1}{2}C_9+C_{10}]$	$\frac{1}{3}V_{tb}V_{ts}^*[2C_5+4C_6+\frac{1}{2}C_7+C_8]$	⋯
$PE_{b2,b4,b6}$	$\frac{1}{3}V_{tb}V_{ts}^*[2C_3-\frac{1}{2}C_4+\frac{1}{2}C_9-\frac{1}{8}C_{10}]$	$\frac{1}{3}V_{tb}V_{ts}^*[2C_5-\frac{1}{2}C_6+\frac{1}{2}C_7-\frac{1}{8}C_8]$	⋯
$PE_{c1,c4,c5,c7}$	$-\frac{1}{3}V_{tb}V_{ts}^*[4C_3+2C_4+C_9+\frac{1}{2}C_{10}]$	$-\frac{1}{3}V_{tb}V_{ts}^*[4C_5+2C_6+C_7+\frac{1}{2}C_8]$	⋯
$PE_{c2,c3,c6}$	$\frac{1}{3}V_{tb}V_{ts}^*[\frac{1}{2}C_3-2C_4+\frac{1}{8}C_9-\frac{1}{2}C_{10}]$	$\frac{1}{3}V_{tb}V_{ts}^*[\frac{1}{2}C_5-2C_6+\frac{1}{8}C_7-\frac{1}{2}C_8]$	⋯
$PE_{d1,d2,d4,d5,d7}$	$\frac{2}{3}V_{tb}V_{ts}^*[-2C_3+2C_4-\frac{1}{2}C_9+\frac{1}{2}C_{10}]$	$\frac{2}{3}V_{tb}V_{ts}^*[-2C_5+2C_6-\frac{1}{2}C_7+\frac{1}{2}C_8]$	⋯
$PE_{d3,d6}$	$\frac{1}{12}V_{tb}V_{ts}^*[2C_3-2C_4+\frac{1}{2}C_9-\frac{1}{2}C_{10}]$	$\frac{1}{12}V_{tb}V_{ts}^*[2C_5-2C_6+\frac{1}{2}C_7-\frac{1}{2}C_8]$	⋯
$PE_{f1,f2}$	$-\frac{1}{3}V_{tb}V_{ts}^*[\frac{5}{2}C_3+2C_4+\frac{5}{8}C_9+\frac{1}{2}C_{10}]$	$-\frac{1}{3}V_{tb}V_{ts}^*[\frac{5}{2}C_5+2C_6+\frac{5}{8}C_7+\frac{1}{2}C_8]$	⋯
PE_{f3}	$\frac{1}{3}V_{tb}V_{ts}^*[2C_3+\frac{5}{2}C_4+\frac{1}{2}C_9+\frac{5}{8}C_{10}]$	$\frac{1}{3}V_{tb}V_{ts}^*[2C_5+\frac{5}{2}C_6+\frac{1}{2}C_7+\frac{5}{8}C_8]$	⋯
PE_{g1}	$-\frac{3}{4}V_{tb}V_{ts}^*[2C_3+\frac{1}{2}C_9]$	$-\frac{3}{4}V_{tb}V_{ts}^*[2C_5+\frac{1}{2}C_7]$	⋯
PE_{g2}	$\frac{3}{4}V_{tb}V_{ts}^*[-2C_3+2C_4-\frac{1}{2}C_9+\frac{1}{2}C_{10}]$	$\frac{3}{4}V_{tb}V_{ts}^*[-2C_5+2C_6-\frac{1}{2}C_7+\frac{1}{2}C_8]$	⋯
PE_{g3}	$\frac{3}{4}V_{tb}V_{ts}^*[2C_4+\frac{1}{2}C_{10}]$	$\frac{3}{4}V_{tb}V_{ts}^*[2C_6+\frac{1}{2}C_8]$	⋯
PE_{g4}	0	0	⋯
$E_{a1-a7,e1-e4,f4}$	$\frac{1}{3}V_{ub}V_{us}^*[C_1-C_2]$	⋯	⋯
$E_{b1,b3,b5,b7}$	$\frac{1}{3}V_{ub}V_{us}^*[C_1+2C_2]$	⋯	⋯
$E_{b2,b4,b6}$	$\frac{1}{3}V_{ub}V_{us}^*[C_1-\frac{1}{4}C_2]$	⋯	⋯
$E_{c1,c4,c5,c7}$	$-\frac{1}{3}V_{ub}V_{us}^*[2C_1+C_2]$	⋯	⋯
$E_{c2,c3,c6}$	$\frac{1}{3}V_{ub}V_{us}^*[\frac{1}{4}C_1-C_2]$	⋯	⋯
$E_{d1,d2,d4,d5,d7}$	$\frac{2}{3}V_{ub}V_{us}^*[-C_1+C_2]$	⋯	⋯
$E_{d3,d6}$	$\frac{1}{12}V_{ub}V_{us}^*[C_1-C_2]$	⋯	⋯
$E_{f1,f2}$	$-\frac{1}{3}V_{ub}V_{us}^*[\frac{5}{4}C_1-C_2]$	⋯	⋯
E_{f3}	$\frac{1}{3}V_{ub}V_{us}^*[C_1+\frac{5}{4}C_2]$	⋯	⋯
E_{g1}	$-\frac{3}{4}V_{ub}V_{us}^*C_1$	⋯	⋯
E_{g2}	$\frac{3}{4}V_{ub}V_{us}^*[-C_1+C_2]$	⋯	⋯
E_{g3}	$\frac{3}{4}V_{ub}V_{us}^*C_2$	⋯	⋯
E_{g4}	0	⋯	⋯
$B_{a1-a4,b1-b4}$	$\frac{1}{4}V_{ub}V_{us}^*[-C_1+C_2]$	⋯	⋯
$PB_{a1-a4,b1-b4}$	$\frac{1}{4}V_{tb}V_{ts}^*[-2C_3+2C_4-\frac{1}{2}C_9+\frac{1}{2}C_{10}]$	⋯	$\frac{1}{4}V_{tb}V_{ts}^*[-2C_5+2C_6-\frac{1}{2}C_7+\frac{1}{2}C_8]$

TABLE X. The virtualities of the internal gluon $t_{A,B}$ and quark $t_{C,D}$ for the exchange topological diagrams.

	R_{ij}	
$\frac{t_A}{M^2}$	$E_{a1-d7,}PE_{a1-d7,}B_{a1-b4,}PB_{a1-b4}$	x_3x_3'
	$E_{e1-e4,f1-f4,}PE_{e1-e4,f1-f4}$	$(1-x_2')(x_3+y-1)$
	$E_{g1-g4,}PE_{g1-g4}$	$x_1'(y-1)$
$\frac{t_B}{M^2}$	$E_{a1,a2,a5-a7,b1,b2,b5-b7,c1-c3,c6,c7,d1-d3,d6,d7,e1-e4,f1-f4,}$ $PE_{a1-a5,b1-b5,c1-c5,d1-d5,e1-e4,f1-f4}$	$x_1'(y-1)$
	$E_{a3,a4,b3,b4,c4,c5,d4,d5,g1-g4,}PE_{a6,a7,b6,b7,c6,c7,d6,d7,g1-g4}$	$(1-x_2')(x_3+y-1)$
	$B_{a1-a4,}PB_{a1-a4}$	$x_3'(x_3+y-1)$
	$B_{b1-b4,}PB_{b1-b4}$	$x_3'(x_3-y)$
$\frac{t_C}{M^2}$	$E_{a1,b1,c1,d1,}PE_{a3,b3,c4,d4}$	$x_3'(1-x_1)$
	$E_{a2,b2,c3,d3,}PE_{a2,b2,c3,d3}$	$x_3'(x_3-y)$
	$E_{a3,b3,c2,c4,d4,}PE_{a6,b4,b6,c4,d6}$	$x_3'(x_3+y-1)$
	$E_{a4,b4,c5,d5,}PE_{a7,b7,c7,d7}$	$x_3(1-x_2')$
	$E_{a5,b5,c6,d6,}PE_{a1,b1,c1,d1}$	$x_3'(1-x_2)+x_2$
	$E_{a6,e4,f4,}PE_{a4,e4,f4}$	x_3+y-1
	$E_{a7,b7,c7,d7,}PE_{a5,b5,c5,d5}$	$x_3(1-x_1')$
	$E_{b6,}PE_{c2}$	$x_1'(x_1+y-1)-x_1-y+2$
	$E_{d2,e2,f2,}PE_{d2,e2,f2}$	$(x_3-1)(1-x_2')$
	$E_{e1,f1,}PE_{e3,f3}$	$(x_1-y)(x_2'-1)$
	$E_{e3,f3,}PE_{e1,f1}$	$x_2'(x_2-y)+1$
	$E_{g1-g4,}PE_{g1-g4}$	x_3x_3'
	$B_{a1-a4,b1-b4,}PB_{a1-a4,b1-b4}$	$x_3'(x_3-1)$
$\frac{t_D}{M^2}$	$E_{a1,a2,a5,a6,}PE_{a1-a4}$	$(x_3'-1)(1-y)$
	$E_{a3,a4,a7,}PE_{a5-a7}$	x_3+y-1
	$E_{b1,b2,b7,}PE_{b3-b5}$	$x_1'(x_1+y-1)-x_1-y+2$
	$E_{b3-b6,g3,}PE_{c1,c2,c6,c7,g1}$	$x_2'(x_2-y)+1$
	$E_{c1,c2,c4,c5,g1,}PE_{b3,b4,b6,b7,g3}$	$(x_1-y)(x_2'-1)$
	$E_{c3,c6,c7,}PE_{b1,b2,b5}$	$x_1'(x_2+y-1)$
	$E_{d1,d2,d6,d7,}PE_{d1,d2,d4,d5}$	$-x_1'$
	$E_{d3-d5,g2,}PE_{d3,d6,d7,g2,}B_{a4,b4,}PB_{a2,b2}$	$(x_3-1)(1-x_2')$
	$E_{e1-e4,}PE_{e1-e4}$	$(1-x_2')(y-1)$
	$E_{f1-f4,}PE_{f1-f4}$	$x_1'(x_3+y-1)$
	$E_{g4,}PE_{g4}$	x_3+y
	$B_{a1,b1,}PB_{a1,b1}$	$x_2(1-x_3')+1$
	$B_{a2,b2,}PB_{a4,b4}$	$(x_3-1)(1-x_1')$
	$B_{a3,b3,}PB_{a3,b3}$	$-x_1x_3'$

TABLE XI. The expressions of $[\mathcal{D}b]$ and $\Omega_{R_{ij}}$ for the exchange topological diagrams.

R_{ij}	$[\mathcal{D}b]$	$\Omega_{R_{ij}}$
E_{a1}, PE_{a3}	$\int d^2\mathbf{b}_2 d^2\mathbf{b}_3 d^2\mathbf{b}_2' d^2\mathbf{b}_3'$	$\frac{1}{(2\pi)^4} K_0(\sqrt{t_A}\lvert\mathbf{b}_2-\mathbf{b}_3\rvert)K_0(\sqrt{t_B}\lvert\mathbf{b}_2'\rvert)K_0(\sqrt{t_C}\lvert\mathbf{b}_2\rvert)K_0(\sqrt{t_D}\lvert\mathbf{b}_2'-\mathbf{b}_3'-\mathbf{b}_3\rvert)$
E_{a2}, PE_{a2}	$\int d^2\mathbf{b}_q d^2\mathbf{b}_3 d^2\mathbf{b}_2' d^2\mathbf{b}_3'$	$\frac{1}{(2\pi)^4} K_0(\sqrt{t_A}\lvert\mathbf{b}_q-\mathbf{b}_3'\rvert)K_0(\sqrt{t_B}\lvert\mathbf{b}_2'\rvert)K_0(\sqrt{t_C}\lvert\mathbf{b}_q-\mathbf{b}_3-\mathbf{b}_3'\rvert)K_0(\sqrt{t_D}\lvert\mathbf{b}_2'-\mathbf{b}_3'-\mathbf{b}_3\rvert)$
E_{a3}, PE_{a6}	$\int d^2\mathbf{b}_q d^2\mathbf{b}_3 d^2\mathbf{b}_2' d^2\mathbf{b}_3'$	$\frac{1}{(2\pi)^4} K_0(\sqrt{t_A}\lvert\mathbf{b}_q-\mathbf{b}_3\rvert)K_0(\sqrt{t_B}\lvert\mathbf{b}_2'\rvert)K_0(\sqrt{t_C}\lvert\mathbf{b}_q-\mathbf{b}_3-\mathbf{b}_3'\rvert)K_0(\sqrt{t_D}\lvert\mathbf{b}_2'-\mathbf{b}_3'-\mathbf{b}_3\rvert)$
E_{a4}, PE_{a7}	$\int d^2\mathbf{b}_q d^2\mathbf{b}_3 d^2\mathbf{b}_2' d^2\mathbf{b}_3'$	$\frac{1}{(2\pi)^4} K_0(\sqrt{t_A}\lvert\mathbf{b}_3-\mathbf{b}_2'\rvert)K_0(\sqrt{t_B}\lvert\mathbf{b}_3-\mathbf{b}_q-\mathbf{b}_2'+\mathbf{b}_3'\rvert)K_0(\sqrt{t_C}\lvert\mathbf{b}_q-\mathbf{b}_3'-\mathbf{b}_3\rvert)K_0(\sqrt{t_D}\lvert\mathbf{b}_2'-\mathbf{b}_3'-\mathbf{b}_3\rvert)$
E_{a5}, PE_{a1}	$\int d^2\mathbf{b}_2 d^2\mathbf{b}_3 d^2\mathbf{b}_2' d^2\mathbf{b}_3'$	$\frac{1}{(2\pi)^4} K_0(\sqrt{t_A}\lvert\mathbf{b}_3\rvert)K_0(\sqrt{t_B}\lvert\mathbf{b}_2'\rvert)K_0(\sqrt{t_C}\lvert\mathbf{b}_2\rvert)K_0(\sqrt{t_D}\lvert\mathbf{b}_2+\mathbf{b}_2'-\mathbf{b}_3'-\mathbf{b}_3\rvert)$
E_{a6}, PE_{a4}	$\int d^2\mathbf{b}_3 d^2\mathbf{b}_2' d^2\mathbf{b}_3'$	$K_0(\sqrt{t_B}\lvert\mathbf{b}_2'\rvert)h_2(\mathbf{b}_2'-\mathbf{b}_3', \mathbf{b}_2'-\mathbf{b}_3'-\mathbf{b}_3, t_A, t_C, t_D)$
E_{a7}, PE_{a5}	$\int d^2\mathbf{b}_3 d^2\mathbf{b}_2' d^2\mathbf{b}_3'$	$K_0(\sqrt{t_A}\lvert\mathbf{b}_2'-\mathbf{b}_3'\rvert)h_2(\mathbf{b}_2'-\mathbf{b}_3'-\mathbf{b}_3, -\mathbf{b}_3-\mathbf{b}_3', t_B, t_C, t_D)$
E_{b1}, PE_{c4}	$\int d^2\mathbf{b}_2 d^2\mathbf{b}_3 d^2\mathbf{b}_2' d^2\mathbf{b}_3'$	$\frac{1}{(2\pi)^4} K_0(\sqrt{t_A}\lvert\mathbf{b}_2-\mathbf{b}_3\rvert)K_0(\sqrt{t_B}\lvert\mathbf{b}_3+\mathbf{b}_3'\rvert)K_0(\sqrt{t_C}\lvert\mathbf{b}_2-\mathbf{b}_3+\mathbf{b}_2'-\mathbf{b}_3'\rvert)K_0(\sqrt{t_D}\lvert\mathbf{b}_2'-\mathbf{b}_3'-\mathbf{b}_3\rvert)$

(Table continued)

TABLE XI. *(Continued)*

R_{ij}	$[\mathcal{D}b]$	$\Omega_{R_{ij}}$
E_{b2}, PE_{c3}	$\int d^2\mathbf{b}_q d^2\mathbf{b}_3 d^2\mathbf{b}'_2 d^2\mathbf{b}'_3$	$\frac{1}{(2\pi)^4} K_0(\sqrt{t_A}\lvert\mathbf{b}_q - \mathbf{b}'_3\rvert) K_0(\sqrt{t_B}\lvert\mathbf{b}_3 + \mathbf{b}'_3\rvert) K_0(\sqrt{t_C}\lvert\mathbf{b}_q - \mathbf{b}'_2\rvert) K_0(\sqrt{t_D}\lvert\mathbf{b}'_2 - \mathbf{b}'_3 - \mathbf{b}_3\rvert)$
E_{b3}, PE_{c6}	$\int d^2\mathbf{b}_q d^2\mathbf{b}_3 d^2\mathbf{b}'_2 d^2\mathbf{b}'_3$	$\frac{1}{(2\pi)^4} K_0(\sqrt{t_A}\lvert\mathbf{b}'_2 - \mathbf{b}'_3 - \mathbf{b}_q\rvert) K_0(\sqrt{t_B}\lvert\mathbf{b}_3 + \mathbf{b}'_3\rvert) K_0(\sqrt{t_C}\lvert\mathbf{b}_q - \mathbf{b}'_2\rvert) K_0(\sqrt{t_D}\lvert\mathbf{b}'_2 - \mathbf{b}'_3 - \mathbf{b}_3\rvert)$
E_{b4}, PE_{c7}	$\int d^2\mathbf{b}_q d^2\mathbf{b}_3 d^2\mathbf{b}'_2 d^2\mathbf{b}'_3$	$\frac{1}{(2\pi)^4} K_0(\sqrt{t_A}\lvert\mathbf{b}'_3\rvert) K_0(\sqrt{t_B}\lvert\mathbf{b}'_2 - \mathbf{b}'_3 - \mathbf{b}_3 - \mathbf{b}_q\rvert) K_0(\sqrt{t_C}\lvert\mathbf{b}_q - \mathbf{b}'_2\rvert) K_0(\sqrt{t_D}\lvert\mathbf{b}'_2 - \mathbf{b}'_3 - \mathbf{b}_3\rvert)$
E_{b5}, PE_{c1}	$\int d^2\mathbf{b}_3 d^2\mathbf{b}'_2 d^2\mathbf{b}'_3$	$K_0(\sqrt{t_A}\lvert\mathbf{b}_3\rvert) h_2(\mathbf{b}'_2 - \mathbf{b}'_3 - \mathbf{b}_3, \mathbf{b}'_2, t_B, t_C, t_D)$
E_{b6}, PE_{c2}	$\int d^2\mathbf{b}_3 d^2\mathbf{b}'_2 d^2\mathbf{b}'_3$	$K_0(\sqrt{t_B}\lvert\mathbf{b}_3 + \mathbf{b}'_3\rvert) h_2(\mathbf{b}'_2 - \mathbf{b}'_3, \mathbf{b}'_2 - \mathbf{b}'_3 - \mathbf{b}_3, t_A, t_C, t_D)$
E_{b7}, PE_{c5}	$\int d^2\mathbf{b}_2 d^2\mathbf{b}_3 d^2\mathbf{b}'_2 d^2\mathbf{b}'_3$	$\frac{1}{(2\pi)^4} K_0(\sqrt{t_A}\lvert\mathbf{b}'_2 - \mathbf{b}'_3\rvert) K_0(\sqrt{t_B}\lvert\mathbf{b}_3 + \mathbf{b}'_3\rvert) K_0(\sqrt{t_C}\lvert\mathbf{b}_2 - \mathbf{b}_3 + \mathbf{b}'_2 - \mathbf{b}'_3\rvert) K_0(\sqrt{t_D}\lvert\mathbf{b}_2\rvert)$
E_{c1}, PE_{b3}	$\int d^2\mathbf{b}'_3 d^2\mathbf{b}_2 d^2\mathbf{b}_3$	$K_0(\sqrt{t_A}\lvert\mathbf{b}_2 - \mathbf{b}_3\rvert) h_2(\mathbf{b}_2, \mathbf{b}_3 + \mathbf{b}'_3, t_B, t_C, t_D)$
E_{c2}, PE_{b4}	$\int d^2\mathbf{b}'_3 d^2\mathbf{b}_2 d^2\mathbf{b}_3$	$K_0(\sqrt{t_A}\lvert\mathbf{b}_2 - \mathbf{b}_3 - \mathbf{b}'_3\rvert) h_2(\mathbf{b}_3, \mathbf{b}_2, t_B, t_C, t_D)$
E_{c3}, PE_{b2}	$\int d^2\mathbf{b}_q d^2\mathbf{b}'_3 d^2\mathbf{b}_2 d^2\mathbf{b}_3$	$\frac{1}{(2\pi)^4} K_0(\sqrt{t_A}\lvert\mathbf{b}_q - \mathbf{b}'_3\rvert) K_0(\sqrt{t_B}\lvert\mathbf{b}_2 - \mathbf{b}_3 - \mathbf{b}'_3\rvert) K_0(\sqrt{t_C}\lvert\mathbf{b}_q - \mathbf{b}_3 - \mathbf{b}'_3\rvert) K_0(\sqrt{t_D}\lvert\mathbf{b}_2\rvert)$
E_{c4}, PE_{b6}	$\int d^2\mathbf{b}_q d^2\mathbf{b}'_3 d^2\mathbf{b}_2 d^2\mathbf{b}_3$	$\frac{1}{(2\pi)^4} K_0(\sqrt{t_A}\lvert\mathbf{b}_q - \mathbf{b}_3\rvert) K_0(\sqrt{t_B}\lvert\mathbf{b}_2 - \mathbf{b}_3 - \mathbf{b}'_3\rvert) K_0(\sqrt{t_C}\lvert\mathbf{b}_q - \mathbf{b}_3 - \mathbf{b}'_3\rvert) K_0(\sqrt{t_D}\lvert\mathbf{b}_2\rvert)$
E_{c5}, PE_{b7}	$\int d^2\mathbf{b}_q d^2\mathbf{b}'_3 d^2\mathbf{b}_2 d^2\mathbf{b}_3$	$\frac{1}{(2\pi)^4} K_0(\sqrt{t_A}\lvert\mathbf{b}'_3\rvert) K_0(\sqrt{t_B}\lvert\mathbf{b}_2 - \mathbf{b}_q\rvert) K_0(\sqrt{t_C}\lvert\mathbf{b}_q - \mathbf{b}_3 - \mathbf{b}'_3\rvert) K_0(\sqrt{t_D}\lvert\mathbf{b}_2\rvert)$
E_{c6}, PE_{b1}	$\int d^2\mathbf{b}_q d^2\mathbf{b}'_3 d^2\mathbf{b}_2 d^2\mathbf{b}_3$	$\frac{1}{(2\pi)^4} K_0(\sqrt{t_A}\lvert\mathbf{b}'_3\rvert) K_0(\sqrt{t_B}\lvert\mathbf{b}_2 - \mathbf{b}_3 - \mathbf{b}'_3\rvert) K_0(\sqrt{t_C}\lvert\mathbf{b}_q - \mathbf{b}_3 - \mathbf{b}'_3\rvert) K_0(\sqrt{t_D}\lvert\mathbf{b}_2 + \mathbf{b}_q - \mathbf{b}_3 - \mathbf{b}'_3\rvert)$
E_{c7}, PE_{b5}	$\int d^2\mathbf{b}_2 d^2\mathbf{b}_3 d^2\mathbf{b}'_2 d^2\mathbf{b}'_3$	$\frac{1}{(2\pi)^4} K_0(\sqrt{t_A}\lvert\mathbf{b}'_2 - \mathbf{b}'_3\rvert) K_0(\sqrt{t_B}\lvert\mathbf{b}_2 - \mathbf{b}_3 - \mathbf{b}'_3\rvert) K_0(\sqrt{t_C}\lvert\mathbf{b}'_2 - \mathbf{b}'_3 + \mathbf{b}_3\rvert) K_0(\sqrt{t_D}\lvert\mathbf{b}_2\rvert)$
E_{d1}, PE_{d4}	$\int d^2\mathbf{b}_2 d^2\mathbf{b}_3 d^2\mathbf{b}'_3 d^2\mathbf{b}_q$	$\frac{1}{(2\pi)^4} K_0(\sqrt{t_A}\lvert\mathbf{b}_2 - \mathbf{b}_3\rvert) K_0(\sqrt{t_B}\lvert\mathbf{b}_q\rvert) K_0(\sqrt{t_C}\lvert\mathbf{b}_2\rvert) K_0(\sqrt{t_D}\lvert\mathbf{b}_q - \mathbf{b}_3 - \mathbf{b}'_3)$
E_{d2}, PE_{d2}	$\int d^2\mathbf{b}_3 d^2\mathbf{b}'_3 d^2\mathbf{b}_q$	$K_0(\sqrt{t_B}\lvert\mathbf{b}_q\rvert) h_2(\mathbf{b}_q - \mathbf{b}'_3, \mathbf{b}_q - \mathbf{b}_3 - \mathbf{b}'_3, t_A, t_C, t_D)$
E_{d3}, PE_{d3}	$\int d^2\mathbf{b}_3 d^2\mathbf{b}'_3 d^2\mathbf{b}_q$	$K_0(\sqrt{t_A}\lvert\mathbf{b}_q - \mathbf{b}'_3\rvert) h_2(\mathbf{b}_3 + \mathbf{b}'_3, \mathbf{b}_q - \mathbf{b}_3 - \mathbf{b}'_3, t_B, t_C, t_D)$
E_{d4}, PE_{d6}	$\int d^2\mathbf{b}_3 d^2\mathbf{b}'_3 d^2\mathbf{b}_q$	$h_3(\mathbf{b}_3 - \mathbf{b}_q, \mathbf{b}_3 + \mathbf{b}'_3 - \mathbf{b}_q, -\mathbf{b}_3 + \mathbf{b}'_3, t_A, t_B, t_C, t_D)$
E_{d5}, PE_{d7}	$\int d^2\mathbf{b}_3 d^2\mathbf{b}'_3 d^2\mathbf{b}_q$	$K_0(\sqrt{t_A}\lvert\mathbf{b}'_3\rvert) K_0(\sqrt{t_B}\lvert\mathbf{b}_q\rvert) h_1(\mathbf{b}_q - \mathbf{b}_3 - \mathbf{b}'_3, t_C, t_D)$
E_{d6}, PE_{d1}	$\int d^2\mathbf{b}_2 d^2\mathbf{b}_3 d^2\mathbf{b}'_3 d^2\mathbf{b}_q$	$\frac{1}{(2\pi)^4} K_0(\sqrt{t_A}\lvert\mathbf{b}_3\rvert) K_0(\sqrt{t_B}\lvert\mathbf{b}_q\rvert) K_0(\sqrt{t_C}\lvert\mathbf{b}_2\rvert) K_0(\sqrt{t_D}\lvert\mathbf{b}_q + \mathbf{b}_2 - \mathbf{b}'_3 - \mathbf{b}_3\rvert)$
E_{d7}, PE_{d5}	$\int d^2\mathbf{b}'_2 d^2\mathbf{b}'_3 d^2\mathbf{b}_3 d^2\mathbf{b}_q$	$\frac{1}{(2\pi)^4} K_0(\sqrt{t_A}\lvert\mathbf{b}'_2 - \mathbf{b}'_3\rvert) K_0(\sqrt{t_B}\lvert\mathbf{b}_q\rvert) K_0(\sqrt{t_C}\lvert\mathbf{b}'_2 - \mathbf{b}'_3 - \mathbf{b}_3\rvert) K_0(\sqrt{t_D}\lvert\mathbf{b}_q - \mathbf{b}_3 - \mathbf{b}'_3\rvert)$
E_{e1}, PE_{e3}	$\int d^2\mathbf{b}_2 d^2\mathbf{b}_3 d^2\mathbf{b}'_3 d^2\mathbf{b}_q$	$\frac{1}{(2\pi)^4} K_0(\sqrt{t_A}\lvert\mathbf{b}_2 - \mathbf{b}_3\rvert) K_0(\sqrt{t_B}\lvert\mathbf{b}'_3\rvert) K_0(\sqrt{t_C}\lvert\mathbf{b}_2\rvert) K_0(\sqrt{t_D}\lvert\mathbf{b}_q - \mathbf{b}_3 - \mathbf{b}'_3\rvert)$
E_{e2}, PE_{e2}	$\int d^2\mathbf{b}'_2 d^2\mathbf{b}'_3 d^2\mathbf{b}_3 d^2\mathbf{b}_q$	$\frac{1}{(2\pi)^4} K_0(\sqrt{t_A}\lvert\mathbf{b}_q + \mathbf{b}_3 - \mathbf{b}'_2\rvert) K_0(\sqrt{t_B}\lvert\mathbf{b}'_3\rvert) K_0(\sqrt{t_C}\lvert\mathbf{b}_q - \mathbf{b}'_2\rvert) K_0(\sqrt{t_D}\lvert\mathbf{b}_3 + \mathbf{b}'_3 - \mathbf{b}'_2\rvert)$
E_{e3}, PE_{e1}	$\int d^2\mathbf{b}'_2 d^2\mathbf{b}'_3 d^2\mathbf{b}_3 d^2\mathbf{b}_q$	$\frac{1}{(2\pi)^4} K_0(\sqrt{t_A}\lvert\mathbf{b}'_3\rvert) K_0(\sqrt{t_B}\lvert\mathbf{b}_q - \mathbf{b}'_2 - \mathbf{b}'_3\rvert) K_0(\sqrt{t_C}\lvert\mathbf{b}_q - \mathbf{b}'_2\rvert) K_0(\sqrt{t_D}\lvert\mathbf{b}_3 + \mathbf{b}'_3 - \mathbf{b}_q\rvert)$
E_{e4}, PE_{e4}	$\int d^2\mathbf{b}'_2 d^2\mathbf{b}'_3 d^2\mathbf{b}_3 d^2\mathbf{b}_q$	$\frac{1}{(2\pi)^4} K_0(\sqrt{t_A}\lvert\mathbf{b}_3 + \mathbf{b}'_2 - \mathbf{b}_q\rvert) K_0(\sqrt{t_B}\lvert\mathbf{b}'_3\rvert) K_0(\sqrt{t_C}\lvert\mathbf{b}_q - \mathbf{b}'_2\rvert) K_0(\sqrt{t_D}\lvert\mathbf{b}_3 + \mathbf{b}'_3 - \mathbf{b}_q\rvert)$
E_{f1}, PE_{f3}	$\int d^2\mathbf{b}'_2 d^2\mathbf{b}'_3 d^2\mathbf{b}_2 d^2\mathbf{b}_3$	$\frac{1}{(2\pi)^4} K_0(\sqrt{t_A}\lvert\mathbf{b}'_2 + \mathbf{b}'_3 - \mathbf{b}_2\rvert) K_0(\sqrt{t_B}\lvert\mathbf{b}_3 - \mathbf{b}'_2\rvert) K_0(\sqrt{t_C}\lvert\mathbf{b}_2\rvert) K_0(\sqrt{t_D}\lvert\mathbf{b}_3 + \mathbf{b}'_3 - \mathbf{b}'_2\rvert)$
E_{f2}, PE_{f2}	$\int d^2\mathbf{b}'_2 d^2\mathbf{b}'_3 d^2\mathbf{b}_3 d^2\mathbf{b}_q$	$\frac{1}{(2\pi)^4} K_0(\sqrt{t_A}\lvert\mathbf{b}_q - \mathbf{b}'_3\rvert) K_0(\sqrt{t_B}\lvert\mathbf{b}_3 - \mathbf{b}'_2\rvert) K_0(\sqrt{t_C}\lvert\mathbf{b}_q - \mathbf{b}'_2\rvert) K_0(\sqrt{t_D}\lvert\mathbf{b}_3 + \mathbf{b}'_3 - \mathbf{b}'_2\rvert)$
E_{f3}, PE_{f1}	$\int d^2\mathbf{b}'_2 d^2\mathbf{b}'_3 d^2\mathbf{b}_2 d^2\mathbf{b}_3$	$\frac{1}{(2\pi)^4} K_0(\sqrt{t_A}\lvert\mathbf{b}_2 + \mathbf{b}'_2 - \mathbf{b}'_3\rvert) K_0(\sqrt{t_B}\lvert\mathbf{b}_3 - \mathbf{b}_2 - \mathbf{b}'_2\rvert) K_0(\sqrt{t_C}\lvert\mathbf{b}_2\rvert) K_0(\sqrt{t_D}\lvert\mathbf{b}_2 - \mathbf{b}_3 + \mathbf{b}'_2 - \mathbf{b}'_3\rvert)$
E_{f4}, PE_{f4}	$\int d^2\mathbf{b}'_2 d^2\mathbf{b}'_3 d^2\mathbf{b}_3 d^2\mathbf{b}_q$	$\frac{1}{(2\pi)^4} K_0(\sqrt{t_A}\lvert\mathbf{b}'_2 - \mathbf{b}'_3\rvert) K_0(\sqrt{t_B}\lvert\mathbf{b}_3 - \mathbf{b}_q\rvert) K_0(\sqrt{t_C}\lvert\mathbf{b}'_2 - \mathbf{b}_q\rvert) K_0(\sqrt{t_D}\lvert\mathbf{b}_3 + \mathbf{b}'_3 - \mathbf{b}_q\rvert)$
E_{g1}, PE_{g3}	$\int d^2\mathbf{b}'_2 d^2\mathbf{b}_2 d^2\mathbf{b}_3$	$K_0(\sqrt{t_D}\lvert\mathbf{b}_2\rvert) h_2(\mathbf{b}_2 - \mathbf{b}_3, \mathbf{b}_2 - \mathbf{b}'_2, t_A, t_B, t_C)$
E_{g2}, PE_{g2}	$\int d^2\mathbf{b}_q d^2\mathbf{b}'_2 d^2\mathbf{b}_3$	$K_0(\sqrt{t_D}\lvert\mathbf{b}_q - \mathbf{b}'_2\rvert) h_2(\mathbf{b}'_2 - \mathbf{b}_3 - \mathbf{b}_q, -\mathbf{b}_q, t_A, t_B, t_C)$
E_{g3}, PE_{g1}	$\int d^2\mathbf{b}'_2 d^2\mathbf{b}_2 d^2\mathbf{b}_3$	$K_0(\sqrt{t_D}\lvert\mathbf{b}_2\rvert) h_2(-\mathbf{b}_3, -\mathbf{b}_2 - \mathbf{b}'_2, t_A, t_B, t_C)$
E_{g4}, PE_{g4}	$\int d^2\mathbf{b}_q d^2\mathbf{b}_3 d^2\mathbf{b}'_3$	$K_0(\sqrt{t_D}\lvert\mathbf{b}_q - \mathbf{b}'_3\rvert) h_2(\mathbf{b}_q - \mathbf{b}_3 - \mathbf{b}'_3, \mathbf{b}_3 + \mathbf{b}'_3, t_A, t_B, t_C)$
B_{a1}, PB_{a1}	$\int d^2\mathbf{b}_q d^2\mathbf{b}_2 d^2\mathbf{b}_3$	$K_0(\sqrt{t_B}\lvert\mathbf{b}_q\rvert) K_0(\sqrt{t_D}\lvert\mathbf{b}_2\rvert) h_1(\mathbf{b}_3 - \mathbf{b}_q, t_A, t_C)$
B_{a2}, PB_{a4}	$\int d^2\mathbf{b}_q d^2\mathbf{b}'_2 d^2\mathbf{b}_3$	$K_0(\sqrt{t_B}\lvert\mathbf{b}_q\rvert) K_0(\sqrt{t_D}\lvert\mathbf{b}'_2\rvert) h_1(\mathbf{b}'_2 + \mathbf{b}_3 - \mathbf{b}_q, t_A, t_C)$
B_{a3}, PB_{a3}	$\int d^2\mathbf{b}_q d^2\mathbf{b}_2 d^2\mathbf{b}'_3$	$K_0(\sqrt{t_B}\lvert\mathbf{b}_q\rvert) K_0(\sqrt{t_D}\lvert\mathbf{b}_2\rvert) h_1(\mathbf{b}'_3 + \mathbf{b}_2 + \mathbf{b}_q, t_A, t_C)$
B_{a4}, PB_{a2}	$\int d^2\mathbf{b}_q d^2\mathbf{b}'_3 d^2\mathbf{b}_3$	$K_0(\sqrt{t_B}\lvert\mathbf{b}_q\rvert) K_0(\sqrt{t_D}\lvert\mathbf{b}_3 + \mathbf{b}'_3\rvert) h_1(\mathbf{b}'_3 + \mathbf{b}_q, t_A, t_C)$
B_{b1}, PB_{b1}	$\int d^2\mathbf{b}_q d^2\mathbf{b}_2 d^2\mathbf{b}_3$	$K_0(\sqrt{t_B}\lvert\mathbf{b}_q\rvert) K_0(\sqrt{t_D}\lvert\mathbf{b}_2\rvert) h_1(\mathbf{b}_3 + \mathbf{b}_q, t_A, t_C)$
B_{b2}, PB_{b4}	$\int d^2\mathbf{b}_q d^2\mathbf{b}'_2 d^2\mathbf{b}_3$	$K_0(\sqrt{t_B}\lvert\mathbf{b}_q\rvert) K_0(\sqrt{t_D}\lvert\mathbf{b}'_2\rvert) h_1(\mathbf{b}'_2 + \mathbf{b}_3 + \mathbf{b}_q, t_A, t_C)$
B_{b3}, PB_{b3}	$\int d^2\mathbf{b}_q d^2\mathbf{b}_2 d^2\mathbf{b}_3$	$K_0(\sqrt{t_B}\lvert\mathbf{b}_q\rvert) K_0(\sqrt{t_D}\lvert\mathbf{b}_2\rvert) h_1(\mathbf{b}_3 - \mathbf{b}_2 + \mathbf{b}_q, t_A, t_C)$
B_{b4}, PB_{b2}	$\int d^2\mathbf{b}_q d^2\mathbf{b}'_2 d^2\mathbf{b}_3$	$K_0(\sqrt{t_B}\lvert\mathbf{b}_q\rvert) K_0(\sqrt{t_D}\lvert\mathbf{b}'_2\rvert) (\mathbf{b}_3 - \mathbf{b}'_2 + \mathbf{b}_q, t_A, t_C)$

TABLE XII. The expressions of $H^{LL,LR,SP}_{R_{ij}}$ in the invariant amplitudes $A_1^{T,L}$ and A_2^L for the diagrams $P_{c7,d6}$ and PE_{b3}.

	$\frac{A_1^T}{16M^4}$	$\frac{A_1^L}{16M^4}$	$\frac{A_2^L}{16M^4}$
$H^{LL}_{P_{c7}}$	$r_\phi\Psi_3^{-+}(r_\Lambda-1)\Phi^T(x_3+y-1)$ $(y-x_2)(\phi_V^a-\phi_V^v)$	$r_\phi\Psi_3^{-+}(r_\Lambda-1)\Phi^T\phi_V(x_2-y)$ (x_3+y-1)	$2r_\phi\phi_V(\Phi^A(-\Psi_4x_2'x_3'r_\Lambda-2(x_3-1)$ $y\Psi_2(r_\Lambda+1)+2x_2\Psi_2(r_\Lambda+1)$ $(x_3+y-1)-2y^2\Psi_2(r_\Lambda+1))+\Phi^T$ $(\Psi_3^{-+}(x_3+y-1)(x_2'r_\Lambda-x_2+y)$ $+x_3'\Psi_3^{+-}(r_\Lambda+1)(y-x_2))$ $+\Psi_4x_2'x_3'r_\Lambda\Phi^V)$
$H^{LR}_{P_{c7}}$	$(r_\Lambda-1)\Phi^T\phi_V^T(\Psi_3^{-+}x_2'(x_3+y-1)$ $+x_3'\Psi_3^{+-}(y+x_2))$	$2(r_\Lambda-1)\Phi^T\phi_V^t(\Psi_3^{-+}x_2'(x_3+y-1)$ $-yx_3'\Psi_3^{+-}+x_2x_3'\Psi_3^{+-})$	$-r_\phi^2\phi_V^s(r_\Lambda\Phi^T(\Psi_3^{-+}+\Psi_3^{+-})(x_2'(x_3+y-1)$ $+x_3'(y-x_2))-2\Psi_4(x_2'(x_3+y-1)(\Phi^A+\Phi^V)$ $+x_3'(x_2-y)(\Phi^A-\Phi^V)))-2\Phi^T\phi_V^t$ $(\Psi_3^{-+}x_2'(x_3+y-1)+x_3'\Psi_3^{+-}(x_2-y))$
$H^{SP}_{P_{c7}}$	$r_\phi\Psi_3^{+-}(r_\Lambda-1)\Phi^T(y-x_2)$ $(x_3+y-1)(\phi_V^a+\phi_V^v)$	$r_\phi\Psi_3^{-+}(r_\Lambda-1)\Phi^T\phi_V$ $(y-x_2)(x_3+y-1)$	$2r_\phi\phi_V(\Phi^A(-\Psi_4x_2'x_3'r_\Lambda-2(x_3-1)y\Psi_2$ $(r_\Lambda+1)+2x_2\Psi_2(r_\Lambda+1)(x_3+y-1)$ $-2y^2\Psi_2(r_\Lambda+1))+\Phi^T(\Psi_3^{-+}x_2'(r_\Lambda+1)$ $(x_3+y-1)+\Psi_3^{+-}(x_2-y)(x_3-x_3'$ $r_\Lambda+y-1))-\Psi_4x_2'x_3'r_\Lambda\Phi^V)$
$H^{LL}_{P_{d6}}$	$-r_\phi\Phi^A(r_\Lambda(\Psi_4(x_2'((2(1-x_2-y)-x_3)$ $\phi_V^a+x_3\phi_V^v)+x_3'(1-x_2-y)(\phi_V^a+\phi_V^v))$ $+2\Psi_2(x_2+y-1)(y-x_1)(\phi_V^a-\phi_V^v))$ $+\Psi_4(1-x_1')(x_2+y-1)(\phi_V^a+\phi_V^v))$ $-\frac{1}{2}r_\phi(1-x_1')r_\Lambda\Phi^T(x_2+y-1)(\phi_V^a+\phi_V^v)$ $(\Psi_3^{-+}+\Psi_3^{+-})+r_\phi\Psi_4\Phi^V(x_2'\phi_V^a(x_3r_\Lambda$ $+x_2+y-1)-x_3'(r_\Lambda-1)(x_2+y-1)$ $(\phi_V^a+\phi_V^v)+x_2'\phi_V^v(-r_\Lambda(2(x_2+y-1)$ $+x_3)+x_2+y-1))$	$\frac{1}{2}r_\phi\phi_V(2\Phi^A(r_\Lambda(\Psi_4x_3'(x_2+y-1)$ $-x_3\Psi_4x_2'+2\Psi_2(x_2+y-1)(y-x_1))$ $+\Psi_4(1-x_1')(1-x_2-y))-(1-x_1')$ $r_\Lambda\Phi^T(x_2+y-1)(\Psi_3^{-+}+\Psi_3^{+-})$ $-2\Psi_4\Phi^V(x_2'(r_\Lambda(2x_2+x_3+2y-2)$ $-x_2-y+1)+x_3'(r_\Lambda-1)(x_2+y-1)))$	$r_\phi\phi_V(-2\Phi^A(\Psi_4x_3'(x_2+y-1)-x_3\Psi_4x_2'$ $+2\Psi_2(x_2+y-1)(y-x_1))+\Phi^T$ $(2(1-x_1')\Psi_3^{+-}(x_2+y-1)-r_\Lambda(\Psi_3^{-+}x_2'$ $(2x_2+x_3+2y-2)+x_3'(x_2+y-1)$ $(\Psi_3^{-+}-\Psi_3^{+-})+x_3x_2'\Psi_3^{+-}))+2\Psi_4\Phi^V$ $(x_2'(2x_2+x_3+2y-2)+$ $x_3'(x_2+y-1)))$
$H^{LR}_{P_{d6}}$	$(x_1'-1)(r_\Lambda-1)(x_2+y-1)\Psi_3^{+-}\Phi^T\phi_V^T$	$(x_1'-1)(r_\Lambda-1)(x_2+y-1)\Psi_3^{+-}\Phi^T\phi_V^t$	$2(1-x_1')\Psi_3^{+-}\Phi^T(x_2+y-1)\phi_V^t$ $-r_\phi^2\phi_V^s(2\Phi^A(2\Psi_2(x_2+y-1)(y-x_1)$ $-\Psi_4(x_2'(2x_2+x_3+2y-2)$ $+x_3'(x_2+y-1)))+r_\Lambda\Phi^T$ $(\Psi_3^{-+}+\Psi_3^{+-})(x_3x_2'-x_3'(x_2+y-1))$ $-2\Psi_4\Phi^V(x_3x_2'-x_3'(x_2+y-1)))$

(Table continued)

TABLE XII. *(Continued)*

	$\frac{A_1^T}{16M^4}$	$\frac{A_1^L}{16M^4}$	$\frac{A_2^L}{16M^4}$
$H_{P_{d6}}^{SP}$	$r_\phi\Psi_4(\phi_V^a(x_3'(r_\Lambda-1)(y-x_1)(\Phi^A-\Phi^V)$ $+(x_1'-1)(\Phi^A((2r_\Lambda-1)(y-x_1)-x_3r_\Lambda)$ $+\Phi^V(y-x_3r_\Lambda-x_1)))+\phi_V^v(x_3'(r_\Lambda-1)$ $(y-x_1)(\Phi^V-\Phi^A)+(x_1'-1)(\Phi^A(y-x_3r_\Lambda-x_1)$ $+\Phi^V((2r_\Lambda-1)(y-x_1)-x_3r_\Lambda))))$ $+2r_\phi\Psi_2\Phi^A(r_\Lambda-1)(y-x_1)(x_2+y-1)(\phi_V^a-\phi_V^v)$ $+\frac{1}{2}r_\phi\Phi^T(-\Psi_3^{+-}r_\Lambda(\phi_V^a-\phi_V^v)(x_3'(y-x_1)$ $+(x_1'-1)(3y-3x_1-2x_3))$ $-\Psi_3^{-+}(y-x_1)(\phi_V^a(r_\Lambda(2x_2-x_2'+2y-2)$ $+2(1-x_2-y))+\phi_V^v(2(1-x_2-y)$ $-r_\Lambda(2x_2-x_2'+2y-2))))$	$\frac{1}{2}r_\phi\phi_V(-2\Phi^A(\Psi_4x_2'(x_3(1-r_\Lambda)+x_2+y-1)$ $+\Psi_4x_3'r_\Lambda(x_2+y-1)$ $+2\Psi_2(r_\Lambda-1)(x_2+y-1)(y-x_1))$ $-\Phi^T(\Psi_3^{-+}(y-x_1)(r_\Lambda(x_2'+2x_2+2y-2)$ $-2(x_2+y-1))+\Psi_3^{+-}r_\Lambda(x_2'(3x_2+x_3+3y-3)$ $+2x_3'(x_2+y-1)))-2\Psi_4\Phi^V(x_2'(r_\Lambda(2x_2$ $+x_3+2y-2)x_1-y)+x_3'r_\Lambda(x_2+y-1)))$	$2r_\phi\phi_V(-\Phi^Ar_\Lambda(\Psi_4x_3'(x_2+y-1)$ $-x_3\Psi_4x_2'+2\Psi_2(x_2+y-1)(y-x_1))$ $+\Psi_3^{-+}\Phi^T(x_2+y-1)(y-x_1)$ $-\Psi_4r_\Lambda\Phi^V(x_2'(2x_2+x_3+2y-2)$ $+x_3'(x_2+y-1)))$
$H_{PE_{b3}}^{LL}$	$(1-x_2')((1-x_1)\Phi^T(\Psi_3^{-+}+\Psi_3^{+-})$ $(r_\Lambda(r_\phi\phi_V^a+r_\phi\phi_V^v-\phi_V^T)+\phi_V^T)$ $-\Psi_4\Phi^Ax_3'r_\Lambda\phi_V^T-\Psi_4x_3'r_\Lambda\Phi^V\phi_V^T)$	$(1-x_2')(\Psi_4x_3'r_\Lambda(-\Phi^A-\Phi^V)\phi_V^t$ $+(1-x_1)\Phi^T(\Psi_3^{-+}+\Psi_3^{+-})$ $(r_\phi r_\Lambda\phi_V-(r_\Lambda-1)\phi_V^t))$	$x_3'(2\Psi_4((x_2'-1)r_\Lambda(\Phi^A+\Phi^V)\phi_V^t-r_\phi\phi_V$ $(\Phi^A-\Phi^V)(r_\Lambda(y+1-x_2'-x_1)-x_1+y)$ $+r_\phi^2r_\Lambda(y-x_1)(\Phi^A+\Phi^V)\phi_V^s)-r_\phi r_\Lambda\Phi^T\phi_V$ $(y-x_1)(\Psi_3^{-+}+\Psi_3^{+-}))+(x_1-1)\Phi^T$ $(\Psi_3^{-+}+\Psi_3^{+-})(2((x_2'-1)\phi_V^t+r_\phi^2(y-x_1)\phi_V^s)$ $-r_\phi r_\Lambda(r_\phi(x_2'+2x_1-2y-1)\phi_V^s-2(x_2'-1)\phi_V))$
$H_{PE_{b3}}^{LR}$	$(x_2'-1)x_3'r_\Lambda(\Phi^A-\Phi^V)\Psi_4\phi_V^T$	$(x_2'-1)x_3'r_\Lambda(\Phi^A-\Phi^V)\Psi_4\phi_V^t$	$-r_\phi^2\phi_V^s(x_3'(y-x_1)(2\Psi_4(r_\Lambda+1)(\Phi^A-\Phi^V)$ $+r_\Lambda\Phi^T(\Psi_3^{-+}+\Psi_3^{+-}))+2(x_1-1)(x_2'-1)$ $r_\Lambda\Phi^T(\Psi_3^{-+}+\Psi_3^{+-}))+2\Psi_4\Phi^A(x_2'-1)$ $x_3'r_\Lambda(r_\phi\phi_V+\phi_V^t)+r_\phi(x_1-1)(x_2'-1)$ $(r_\Lambda+2)\Phi^T\phi_V(\Psi_3^{-+}+\Psi_3^{+-})$ $-2\Psi_4(x_2'-1)x_3'r_\Lambda\Phi^V(\phi_V^t-r_\phi\phi_V)$

[1] R. Aaij *et al.* (LHCb Collaboration), Measurement of the differential branching fraction of the decay $\Lambda_b^0 \to \Lambda\mu^+\mu^-$, Phys. Lett. B **725**, 25 (2013).

[2] T. Aaltonen *et al.* (CDF Collaboration), Observation of the Baryonic Flavor-Changing Neutral Current Decay $\Lambda_b \to \Lambda\mu^+\mu^-$, Phys. Rev. Lett. **107**, 201802 (2011).

[3] R. Aaij *et al.* (LHCb Collaboration), First Observation of the Radiative Decay $\Lambda_b^0 \to \Lambda\gamma$, Phys. Rev. Lett. **123**, 031801 (2019).

[4] R. Aaij *et al.* (LHCb Collaboration), Search for the $\Lambda_b^0 \to \Lambda\eta'$ and $\Lambda_b^0 \to \Lambda\eta$ decays with the LHCb detector, J. High Energy Phys. 09 (2015) 006.

[5] R. Aaij *et al.* (LHCb Collaboration), Observation of the $\Lambda_b^0 \to \Lambda\phi$ decay, Phys. Lett. B **759**, 282 (2016).

[6] R. Aaij *et al.* (LHCb Collaboration), Observations of $\Lambda_b^0 \to \Lambda K^+\pi^-$ and $\Lambda_b^0 \to \Lambda K^+K^-$ decays and searches for other Λ_b^0 and Ξ_b^0 decays to $\Lambda h^+h'^-$ final states, J. High Energy Phys. 05 (2016) 081.

[7] R. L. Workman *et al.* (Particle Data Group), Review of particle physics, Prog. Theor. Exp. Phys. **2022**, 083C01 (2022).

[8] J. Zhu, Z. T. Wei, and H. W. Ke, Semileptonic and nonleptonic weak decays of Λ_b^0, Phys. Rev. D **99**, 054020 (2019).

[9] C. Q. Geng, Y. K. Hsiao, Y. H. Lin, and Y. Yu, Study of $\Lambda_b \to \Lambda(\phi, \eta^{(\prime)})$ and $\Lambda_b \to \Lambda K^+K^-$ decays, Eur. Phys. J. C **76**, 399 (2016).

[10] Y. K. Hsiao, Y. Yao, and C. Q. Geng, Charmless two-body anti-triplet b-baryon decays, Phys. Rev. D **95**, 093001 (2017).

[11] C. Q. Geng and C. W. Liu, Time-reversal asymmetries and angular distributions in $\Lambda_b \to \Lambda V$, J. High Energy Phys. 11 (2021) 104.

[12] W. Bensalem, A. Datta, and D. London, T violating triple product correlations in charmless Λ_b decays, Phys. Lett. B **538**, 309 (2002).

[13] W. Bensalem, A. Datta, and D. London, New physics effects on triple product correlations in Λ_b decays, Phys. Rev. D **66**, 094004 (2002).

[14] Z. J. Ajaltouni, E. Conte, and O. Leitner, Λ_b decays into Λ-Vector, Phys. Lett. B **614**, 165 (2005).

[15] O. Leitner, Z. J. Ajaltouni, and E. Conte, An angular distribution analysis of Λ_b decays, Nucl. Phys. **A755**, 435 (2005).

[16] O. Leitner, Z. J. Ajaltouni, and E. Conte, Testing fundamental symmetries with $\Lambda_b \to \Lambda$-Vector decay, arXiv:hep-ph/0602043.

[17] O. Leitner and Z. J. Ajaltouni, Testing *CP* and time reversal symmetries with $\Lambda_b \to \Lambda V(1^-)$ decays, Nucl. Phys. B, Proc. Suppl. **174**, 169 (2007).

[18] M. Gronau and J. L. Rosner, Triple product asymmmetries in Λ_b and Ξ_b decays, Phys. Lett. B **749**, 104 (2015).

[19] G. Durieux, CP violation in multibody decays of beauty baryons, J. High Energy Phys. 10 (2016) 005.

[20] C. W. Liu and C. Q. Geng, Sizable time-reversal violating effects in bottom baryon decays, J. High Energy Phys. 01 (2022) 128.

[21] R. Mohanta, A. K. Giri, and M. P. Khanna, Charmless two-body hadronic decays of Λ_b baryon, Phys. Rev. D **63**, 074001 (2001).

[22] T. Uppal, R. C. Verma, and M. P. Khanna, Constituent quark model analysis of weak mesonic decays of charm baryons, Phys. Rev. D **49**, 3417 (1994).

[23] J. G. Korner and M. Kramer, Exclusive nonleptonic charm baryon decays, Z. Phys. C **55**, 659 (1992).

[24] H. Y. Cheng, Nonleptonic weak decays of bottom baryons, Phys. Rev. D **56**, 2799 (1997); **99**, 079901(E) (2019).

[25] M. Ablikim *et al.* (BESIII Collaboration), Measurements of absolute branching fractions for $\Lambda_c^+ \to \Xi^0 K^+$ and $\Xi(1530)^0 K^+$, Phys. Lett. B **783**, 200 (2018).

[26] N. Sharma and R. Dhir, Estimates of W-exchange contributions to Ξ_{cc} decays, Phys. Rev. D **96**, 113006 (2017).

[27] R. Dhir and N. Sharma, Weak decays of doubly heavy charm Ω_{cc}^+ baryon, Eur. Phys. J. C **78**, 743 (2018).

[28] Q. P. Xu and A. N. Kamal, Cabibbo favored nonleptonic decays of charmed baryons, Phys. Rev. D **46**, 270 (1992).

[29] P. Zenczykowski, Nonleptonic charmed baryon decays: Symmetry properties of parity violating amplitudes, Phys. Rev. D **50**, 5787 (1994).

[30] K. K. Sharma and R. C. Verma, A Study of weak mesonic decays of Λ_c and Ξ_c baryons on the basis of HQET results, Eur. Phys. J. C **7**, 217 (1999).

[31] H. Y. Cheng and B. Tseng, Cabibbo allowed nonleptonic weak decays of charmed baryons, Phys. Rev. D **48**, 4188 (1993).

[32] H. Y. Cheng, X. W. Kang, and F. Xu, Singly Cabibbo-suppressed hadronic decays of Λ_c^+, Phys. Rev. D **97**, 074028 (2018).

[33] J. Zou, F. Xu, G. Meng, and H. Y. Cheng, Two-body hadronic weak decays of antitriplet charmed baryons, Phys. Rev. D **101**, 014011 (2020).

[34] S. Groote and J. G. Körner, Topological tensor invariants and the current algebra approach: Analysis of 196 nonleptonic two-body decays of single and double charm baryons—a review, Eur. Phys. J. C **82**, 297 (2022).

[35] L. J. Jiang, B. He, and R. H. Li, Weak decays of doubly heavy baryons: $\mathcal{B}_{cc} \to \mathcal{B}_c V$, Eur. Phys. J. C **78**, 961 (2018).

[36] F. S. Yu, H. Y. Jiang, R. H. Li, C. D. Lü, W. Wang, and Z. X. Zhao, Discovery potentials of doubly charmed baryons, Chin. Phys. C **42**, 051001 (2018).

[37] H. J. Zhao, Y. L. Wang, Y. K. Hsiao, and Y. Yu, A diagrammatic analysis of two-body charmed baryon decays with flavor symmetry, J. High Energy Phys. 02 (2020) 165.

[38] T. Gutsche, M. A. Ivanov, J. G. Körner, V. E. Lyubovitskij, and Z. Tyulemissov, *Ab initio* three-loop calculation of the W-exchange contribution to nonleptonic decays of double charm baryons, Phys. Rev. D **99**, 056013 (2019).

[39] Y. K. Hsiao, S. Y. Tsai, C. C. Lih, and E. Rodrigues, Testing the W-exchange mechanism with two-body baryonic B decays, J. High Energy Phys. 04 (2020) 035.

[40] M. A. Ivanov, J. G. Korner, V. E. Lyubovitskij, and A. G. Rusetsky, Exclusive nonleptonic decays of bottom and charm baryons in a relativistic three quark model: Evaluation of nonfactorizing diagrams, Phys. Rev. D **57**, 5632 (1998).

[41] M. A. Ivanov, J. G. Korner, V. E. Lyubovitskij, and A. G. Rusetsky, Exclusive nonleptonic bottom to charm baryon decays including nonfactorizable contributions, Mod. Phys. Lett. A **13**, 181 (1998).

[42] Fayyazuddin, W-exchange contribution in hadronic decays of bottom baryon, arXiv:2210.10017.

[43] C. H. Chou, H. H. Shih, S. C. Lee, and H. n. Li, $\Lambda_b \to \Lambda J/\psi$ decay in perturbative QCD, Phys. Rev. D **65**, 074030 (2002).

[44] H. H. Shih, S. C. Lee, and H. n. Li, The $\Lambda_b \to p l\bar{\nu}$ decay in perturbative QCD, Phys. Rev. D **59**, 094014 (1999).

[45] H. H. Shih, S. C. Lee, and H. n. Li, Applicability of perturbative QCD to $\Lambda_b \to \Lambda_c$ decays, Phys. Rev. D **61**, 114002 (2000).

[46] H. H. Shih, S. C. Lee, and H. N. Li, Asymmetry parameter in the polarized $\Lambda_b \to \Lambda_c l\bar{\nu}$ decay, Chin. J. Phys. **39**, 328 (2001), https://inspirehep.net/literature/565648.

[47] X. G. He, T. Li, X. Q. Li, and Y. M. Wang, PQCD calculation for $\Lambda_b \to \Lambda\gamma$ in the standard model, Phys. Rev. D **74**, 034026 (2006).

[48] C. D. Lu, Y. M. Wang, H. Zou, A. Ali, and G. Kramer, Anatomy of the pQCD approach to the baryonic decays $\Lambda_b \to p\pi, pK$, Phys. Rev. D **80**, 034011 (2009).

[49] J. J. Han, Y. Li, H. n. Li, Y. L. Shen, Z. J. Xiao, and F. S. Yu, $\Lambda_b \to p$ transition form factors in perturbative QCD, Eur. Phys. J. C **82**, 686 (2022).

[50] C. Q. Zhang, J. M. Li, M. K. Jia, and Z. Rui, Nonleptonic two-body decays of $\Lambda_b \to \Lambda_c\pi, \Lambda_c K$ in the perturbative QCD approach, Phys. Rev. D **105**, 073005 (2022).

[51] Z. Rui, C. Q. Zhang, J. M. Li, and M. K. Jia, Investigating the color-suppressed decays $\Lambda_b \to \Lambda\psi$ in the perturbative QCD approach, Phys. Rev. D **106**, 053005 (2022).

[52] G. Buchalla, A. J. Buras, and M. E. Lautenbacher, Weak decays beyond leading logarithms, Rev. Mod. Phys. **68**, 1125 (1996).

[53] P. Ball, V. M. Braun, and E. Gardi, Distribution amplitudes of the Λ_b baryon in QCD, Phys. Lett. B **665**, 197 (2008).

[54] A. Ali, C. Hambrock, and A. Y. Parkhomenko, Light-cone wave functions of heavy baryons, Theor. Math. Phys. **170**, 2 (2012).

[55] G. Bell, T. Feldmann, Y. M. Wang, and M. W. Y. Yip, Light-Cone distribution amplitudes for heavy-quark hadrons, J. High Energy Phys. 11 (2013) 191.

[56] Y. M. Wang and Y. L. Shen, Perturbative corrections to $\Lambda_b \to \Lambda$ form factors from QCD light-cone sum rules, J. High Energy Phys. 02 (2016) 179.

[57] A. Ali, C. Hambrock, A. Y. Parkhomenko, and W. Wang, Light-Cone distribution amplitudes of the ground state bottom baryons in HQET, Eur. Phys. J. C **73**, 2302 (2013).

[58] V. M. Braun, S. E. Derkachov, and A. N. Manashov, Integrability of the evolution equations for heavy-light baryon distribution amplitudes, Phys. Lett. B **738**, 334 (2014).

[59] S. Groote, J. G. Korner, and O. I. Yakovlev, An analysis of diagonal and nondiagonal QCD sum rules for heavy baryons at next-to-leading order in α_s, Phys. Rev. D **56**, 3943 (1997).

[60] V. L. Chernyak, A. A. Ogloblin, and I. R. Zhitnitsky, Wave functions of octet baryons, Z. Phys. C **42**, 569 (1989).

[61] Y. M. Wang, Y. Li, and C. D. Lu, Rare Decays of $\Lambda_b \to \Lambda\gamma$ and $\Lambda_b \to \Lambda l^+ l^-$ in the Light-cone Sum Rules, Eur. Phys. J. C **59**, 861 (2009).

[62] Y. L. Liu, C. Y. Cui, and M. Q. Huang, Higher order light-cone distribution amplitudes of the Λ baryon, Eur. Phys. J. C **74**, 3041 (2014).

[63] Y. L. Liu and M. Q. Huang, Distribution amplitudes of Σ and Λ and their electromagnetic form factors, Nucl. Phys. **A821**, 80 (2009).

[64] G. S. Bali, V. M. Braun, M. Göckeler, M. Gruber, F. Hutzler, A. Schäfer, R. W. Schiel, J. Simeth, W. Söldner, and A. Sternbeck *et al.*, Light-cone distribution amplitudes of the baryon octet, J. High Energy Phys. 02 (2016) 070.

[65] V. M. Braun, S. Collins, B. Gläßle, M. Göckeler, A. Schäfer, R. W. Schiel, W. Söldner, A. Sternbeck, and P. Wein, Light-cone distribution amplitudes of the nucleon and negative parity nucleon resonances from Lattice QCD, Phys. Rev. D **89**, 094511 (2014).

[66] G. S. Bali *et al.* (RQCD Collaboration), Light-cone distribution amplitudes of octet baryons from lattice QCD, Eur. Phys. J. A **55**, 116 (2019).

[67] P. Ball, V. M. Braun, Y. Koike, and K. Tanaka, Higher twist distribution amplitudes of vector mesons in QCD: Formalism and twist-three distributions, Nucl. Phys. **B529**, 323 (1998).

[68] P. Ball and V. M. Braun, Higher twist distribution amplitudes of vector mesons in QCD: Twist—4 distributions and meson mass corrections, Nucl. Phys. **B543**, 201 (1999).

[69] P. Ball and G. W. Jones, Twist-3 distribution amplitudes of K^* and phi mesons, J. High Energy Phys. 03 (2007) 069.

[70] Z. Rui, Y. Li, and Z. J. Xiao, Branching ratios, CP asymmetries and polarizations of $B \to \psi(2S)V$ decays, Eur. Phys. J. C **77**, 610 (2017).

[71] M. Ablikim *et al.* (BESIII Collaboration), Polarization and entanglement in baryon-antibaryon pair production in electron-positron annihilation, Nat. Phys. **15**, 631 (2019).

[72] Z. Rui, Y. Li, and H. n. Li, Four-body decays $B_{(s)} \to (K\pi)_{S/P}(K\pi)_{S/P}$ in the perturbative QCD approach, J. High Energy Phys. 05 (2021) 082.

[73] C. Q. Zhang, J. M. Li, M. K. Jia, Y. Li, and Z. Rui, CP-violating observables in four-body $B \to \phi(\to K\bar{K})K^*(\to K\pi)$ decays, Phys. Rev. D **105**, 053002 (2022).

[74] R. Aaij *et al.* (LHCb Collaboration), Measurements of the $\Lambda_b^0 \to J/\psi\Lambda$ decay amplitudes and the Λ_b^0 polarisation in pp collisions at $\sqrt{s} = 7$ TeV, Phys. Lett. B **724**, 27 (2013).

[75] A. Ali, G. Kramer, Y. Li, C. D. Lu, Y. L. Shen, W. Wang, and Y. M. Wang, Charmless non-leptonic B_s decays to PP, PV and VV final states in the pQCD approach, Phys. Rev. D **76**, 074018 (2007).

[76] W. Bensalem, A. Datta, and D. London, New physics effects on triple product correlations in Λ_b decays, Phys. Rev. D **66**, 094004 (2002).

[77] Y. Amhis *et al.* (HFLAV Collaboration), Averages of b-hadron, c-hadron, and τ-lepton properties as of 2021, arXiv:hep-ex/2206.07501.

[78] D. G. Ireland, M. Döring, D. I. Glazier, J. Haidenbauer, M. Mai, R. Murray-Smith, and D. Rönchen, Kaon Photoproduction and the Λ Decay Parameter α_-, Phys. Rev. Lett. **123**, 182301 (2019).

[79] R. Aaij *et al.* (LHCb Collaboration), Measurement of the $\Lambda_b^0 \to J/\psi\Lambda$ angular distribution and the Λ_b^0 polarisation in pp collisions, J. High Energy Phys. 06 (2020) 110.

[80] A. M. Sirunyan *et al.* (CMS Collaboration), Measurement of the Λ_b polarization and angular parameters in $\Lambda_b \to J/\psi\Lambda$ decays from pp collisions at $\sqrt{s} = 7$ and 8 TeV, Phys. Rev. D **97**, 072010 (2018).

[81] G. Aad *et al.* (ATLAS Collaboration), Measurement of the parity-violating asymmetry parameter α_b and the helicity amplitudes for the decay $\Lambda_b^0 \to J/\psi + \Lambda^0$ with the ATLAS detector, Phys. Rev. D **89**, 092009 (2014).

[82] G. Hiller, M. Knecht, F. Legger, and T. Schietinger, Photon polarization from helicity suppression in radiative decays of polarized Λ_b to spin-3/2 baryons, Phys. Lett. B **649**, 152 (2007).